Wiley
Journal of Nanotechnology
Volume 2025, Article ID 5162847, 21 pages
https://doi.org/10.1155/jnt/5162847

WILEY

*Research Article*

# Nanoformulation and Preclinical Evaluation of Dihydroartemisinin–Lumefantrine and Primaquine as Combined Antimalarial Therapy

**Pesila Odera**,[1] **Geoffrey Otieno**,[1] **Joab Onyango**,[1] **Bernhards Ogutu**,[2,3] **James Owour**,[1] **Florence Oloo**,[1,3] **Martin Ongas**,[3] **Hulda Swai**,[4] **and Jeremiah Gathirwa**[2]

[1]*School of Chemistry and Material Science, Technical University of Kenya, Nairobi, Kenya*
[2]*Centre of Traditional Medicine and Drug Research and Centre for Clinical Research, Kenya Medical Research Institute, Nairobi, Kenya*
[3]*Centre for Research in Therapeutic Sciences, Strathmore University Medical Centre, Nairobi, Kenya*
[4]*Africa Center of Excellence CREATES, Nelson Mandela African Institution of Science and Technology (NM-AIST), Arusha, Tanzania*

Correspondence should be addressed to Pesila Odera; oderapesila1@gmail.com

Received 19 July 2024; Accepted 9 April 2025

Academic Editor: Arnab Biswas



The World Health Organization recommends artemisinin-based combinations for uncomplicated malaria treatment. Artemether and lumefantrine (LUM) are the first-line treatments, with artemether serving as a prodrug of dihydroartemisinin (DHA), while primaquine (PQ) is primarily used as a prophylactic drug. However, these drugs face challenges such as toxicity, low bioavailability, and poor aqueous solubility. The advent of nanomedicine offers solutions by improving drug pharmacokinetic and pharmacodynamic profiles, thereby enhancing therapeutic efficacy. This study aimed to improve the efficacy of DHA, LUM, and PQ through nanoformulation using solid lipid nanoparticles (SLNs). These nanoparticles were prepared using a modified solvent extraction method based on a water-in-oil-in-water (W/O/W) double emulsion. The resulting nanoparticles had a mean particle size of 357.1 ± 57.14 nm, a polydispersity index of 0.657 ± 0.091, and a zeta potential of −35.7 ± 1.25 mV. The encapsulation efficiencies of DHA, LUM, and PQ were 93.98 ± 0.41%, 42.03 ± 9.46%, and 87.60 ± 0.64%, respectively, with drug loading capacities of 11.87 ± 0.04%, 24.10 ± 2.88%, and 8.01 ± 0.09%. The drugs followed Kors–Peppas and Higuchi drug release models and were released progressively over 68 h. The nanoparticles were spherically shaped, and Fourier transform infrared (FTIR) spectroscopy confirmed the successful nanoformulation process. The nanoformulated drugs demonstrated 30% greater efficacy than conventional oral doses in clearing *Plasmodium berghei* infection in Swiss albino mice.

**Keywords:** malaria; pharmacokinetics; solid lipid nanoparticles (SLNs); triple-drug nanoformulation

## 1. Introduction

Malaria is a deadly disease of a significant public health concern prevalent in developing countries, particularly affecting children under five and expectant mothers in Africa [1]. Approximately 90% of global malaria-related infections and deaths are attributed to *Plasmodium falciparum* [2, 3]. The World Health Organization (WHO) currently recommends artemisinin-based combination therapies (ACTs) for treating both complicated and uncomplicated malaria [4, 5]. These recommended antimalarials typically combine an artemisinin-based drug with another antimalarial partner drug. Artemether–lumefantrine (LUM) and artesunate-based therapies are the first-line treatments for uncomplicated and complicated malaria, respectively [6].

The WHO has registered several artemisinin-based combinations, including artemether–LUM, dihydroartemisinin (DHA)–piperaquine, artesunate–sulfadoxine–pyrimethamine, artesunate–amodiaquine, and artesunate–mefloquine [7]. Beyond binary drug combinations, triple antimalarial therapies have been developed to enhance parasite clearance and have demonstrated greater efficacy compared to monotherapies or double therapies [8, 9]. Notable examples of triple antimalarial drugs include mefloquine–sulfadoxine–pyrimethamine, which has shown superior antimalarial activity compared to mefloquine alone or sulfadoxine–pyrimethamine alone [10]. Other triple combinations reported in the literature include chloroquine–sulfadoxine–pyrimethamine [11], amodiaquine–sulfadoxine–pyrimethamine [12], artemether–sulfadoxine–pyrimethamine [13], and DHA–piperaquine–primaquine (PQ) [14].

The WHO recommends that PQ be administered alongside ACTs in regions nearing malaria elimination to mitigate artemisinin resistance [8, 15, 16]. Drug combinations are crucial in combating malaria, especially with the emergence of chloroquine-resistant *P. vivax* and *P. falciparum* parasites. Effective combinations consider drugs with different elimination half-lives and mechanisms of action [17, 18]. The inclusion of existing ACTs in triple-drug combinations is necessary to enhance efficacy and target multiple metabolic pathways or stages of the malaria parasite. Advantages of triple-drug combinations include enhanced synergy between medications, simplified administration regimens, and increased efficacy against multidrug-resistant strains [18, 19].

Single-drug regimens have been associated with the development of resistance, such as antibiotic resistance to nitroimidazoles and macrolides [20, 21] and microbial resistance in human immunodeficiency virus (HIV) treatment [22]. Therefore, combining multiple drugs in malaria treatment is essential for overcoming resistance and improving therapeutic outcomes. Triple-drug nanoformulations have proven successful in managing HIV [23] and cancer [24] and in eradicating *Helicobacter pylori* (*H. pylori*) [21].

Antimalarial drugs, whether in binary or triple combinations, face intrinsic challenges such as low bioavailability due to poor solubility; for instance, DHA has an oral bioavailability of just 45% [25]. PQ's toxicity also leads to poor patient compliance [26]. Additionally, current ACTs are encountering partial resistance, posing a significant threat to malaria control efforts [27]. Mismatched pharmacokinetics further reduce the efficacy of combined antimalarial therapies [28].

The advent of nanomedicine has enabled significant improvements in drug pharmacokinetics [29], safety, and oral bioavailability [30]. Nanoparticles (NPs) such as nanosponges, nanospheres, liposomes, nanocapsules, hydrogels, and ethosomes have been functionalized to enhance antimalarial drug activity [31]. These NPs improve drug release profiles and enhance antimalarial efficacy [32]. Liposomes, widely used for pharmaceutical delivery, offer several advantages, including protecting active pharmaceutical ingredients (APIs) from the harsh gastrointestinal environment, reducing toxicity, enabling controlled drug release, and improving biocompatibility and bioavailability [33].

Solid lipid nanoparticles (SLNs), a category of liposomes, have been extensively applied in antimalarial drug delivery [31]. Muga et al. [34] demonstrated that chloroquine nanoformulated with heparin exhibited superior antimalarial activity against the chloroquine-resistant W2 strain compared to free chloroquine. Heparin, a glycosaminoglycan, targets the circumsporozoite protein on sporozoites during the early liver stage of malaria infection [35, 36]. Heparin binds to malaria-infected red blood cells (plasmodium-infected red blood cells [pRBCs]), thereby mitigating malaria severity [37, 38]. Nanoformulation has been successfully applied to various antimalarial drugs, such as PQ [39], DHA [40], quinine [41], and chloroquine [34]. These nanoformulations enhance antimalarial activity and reduce the toxicity of drugs like quinine and PQ [42].

## 2. Materials and Methods

*2.1. Materials.* Stearic acid (SA), acetic acid, chitosan low-viscous (CLV), ethyl acetate (EtOAc), polyvinyl alcohol (PVA) with a molecular weight of 13,000–23,000, D-lactose monohydrate (DLM), and low molecular weight heparin sodium salt (> 180 USP units/mg) were purchased from Sigma-Aldrich in South Africa. The analytical grade chemical products used in this research included EtOAc and acetic acid. SA was used as the lipid matrix in this work. PVA acted as the key emulsions' stabilizer and surfactant. DLM was used as a binder to initiate further NP size reduction and as a probable agent to keep up the blood osmotic balance. Chitosan was applied as a mucoadhesive to improve the circulation and residence time of the NPs in the intestines. Acetonitrile, methanol HPLC grades, dichloromethane, formic acid, and ammonium formate were used as mobile phases in liquid chromatography–mass spectrometer (LC/MS) (Agilent Technologies 6410-Triple Quad LC/MS). The LC/MS used in the research was accessed at a research laboratory in the Center for Research in Therapeutic Sciences, Strathmore University. Deionized water was obtained from a Thermo Scientific water deionizer, while pure standards including heparin sodium salt, PQ, LUM, mefloquine, and DHA were obtained from Sigma-Aldrich. The equipment used for drug nanoformulation was available at the Chemistry Laboratory of the Centre for Traditional Medicine and Drug Research (CTMDR). These included a sonicator (KERRY), high-speed centrifuge (EBA 200), high-speed homogenizer with maximum rotations per minute (rpm) of 10,000 (Silverson L5-MA), hot plate magnetic stirrer with maximum rpm of 6000, zetasizer (Malvern Zetasizer Nano ZSP), and a bench-top Buchi mini spray-dryer (model BUCHI Mini Spray Dryer B-290) accompanied with B-296 Dehumidifier. The scanning electron microscopy (SEM, Quanta FEG 250, FEI) equipment that was used to study the NP morphology was outsourced at the National Research Centre, Egypt. The NP chemical structures were studied using a Fourier transform infrared (FTIR) spectrometer (JASCO 4700 ATR-FT/IR), which was

accessed from the School of Pharmacy and Health Sciences, Technical University of Kenya (TUK). Sodium lauryl sulfate (SLS), acetate buffer, pH meter, and dialysis membrane bags (MWCO: 12–14 kDa) were obtained locally from the CTMDR's chemistry laboratory. A shaker-incubator equipment was accessed in the Production Unit Laboratory at KEMRI. All the nanoformulation excipients and reagents were used as received.

*2.2. Preparation of SLNs.* The emulsion solvent evaporation technique was applied for the preparation of the SLNs. The NPs were prepared by adopting a method used by Omwoyo et al. [40] with minor adjustments. The formulation's organic phase consisted of 50 mg of SA dissolved in 10 mL EtOAc. Additionally, 10, 15, and 60 mg of DHA, PQ, and LUM were added to the above organic phase, respectively. The aqueous phase on the other hand was prepared into a mixture of 1 mL, 1% (w/v) heparin, 10 mL, 2% (w/v) PVA, 5 mL, 0.3% (w/v) CLV, and 5 mL, 5% (w/v) DLM. Emulsification of the resultant oil-in-water (O/W) emulsion was performed using a high-speed homogenization with speeds varied between 8000 and 10,000 rpm for 15 min. The preparation of the NPs is initiated by high-speed homogenization which provides the necessary energy [43]. Effective particle dispersion occurs during homogenization by the solvent extraction process resulting in the formation of NPs with smaller sizes [44]. An increase in homogenization time further reduces the NP size as a result of the effective dispersion of the NPs [43]. The resultant W/O/W double emulsion was directly fed into a bench-top Buchi mini spray dryer and spray-dried under the following spray-drying conditions; atomizing pressure ranged between 4 and 7 bars while spray-drying temperature ranged between 90°C and 120°C. Characterization parameters included particle size (PS), particle charges (zeta potential), polydispersity index (PDI), drug loading (DL%), encapsulation efficiency (EE %), morphology, structure, and antimalarial activity. Nanoformulation conditions were optimized using a two-factorial design. The conditions varied during optimization were homogenization time (10 and 15 min), homogenization speed (8000 and 10,000 rpm), matrix concentration, surfactant concentrations, and types.

## 3. Characterization of the NPs

*3.1. PS Analysis.* The zeta potential, PS, and particle PDI were determined using the dynamic laser scattering (DLS) or photon correlation spectrometer on a zetasizer nano-computerized system. The measurements were made in triplicate, and the data values were recorded as means and standard deviations (mean ± std dev). The colloidal physical stability of the system and the NP surface charge were represented by the NP zeta potential. The measurements were conducted at an angle of 173°, at room temperature (25°C). For measurement purposes, 2 mg of NPs was suspended in distilled water, vortexed, and sonicated to give a suitable scattering intensity. The sonicated samples were placed in three different sets of zetasizer cells and cuvettes ready for analysis.

*3.2. Storage Stability of Studies of DHA–PQ–LUM SLNs.* The International Conference on Harmonisation (ICH) guidelines Q1 (R2) were adopted to assess the stability of the nanoformulated drug samples (ICH Q1A [45]). The samples' stability study was conducted by varying the storage temperatures of the NPs. The NPs were stored for a period of 4 months in cold and room temperatures of 4°C and 25°C, respectively. The NP size, PDI, and zeta potential were determined periodically at time intervals of 0, 1, 2, 3–16 weeks of storage. 1 mg of the NP samples was suspended in distilled water, vortexed using a Cole-Parmer vortex (VM3), and sonicated (KERRY) for about 4 min ready for zetasizer analysis.

*3.3. NP Morphology.* The topography and morphology of the triple nanoformulated samples were analyzed using an SEM (Quanta FEG 250, FEI). The samples were coated with a thin layer of gold by spattering the glazing unit to minimize the heating effect resulting from high-power magnification. The SEM micrographs of the triple nanoformulated drug particles were then captured and recorded.

*3.4. EE and DL.* The EE and DL of the triple nanoformulated drugs were determined using an LC/MS (Agilent Technologies 6410-Triple Quad LC/MS). The NP samples were prepared for LC/MS analysis by making adjustments to the method used in [46]. Briefly, 10 mg of the nanoformulated drug samples was dispersed in 5 mL of deionized water and sonicated for 3 min till full dispersion of the NPs. The resultant solution was then ultracentrifuged (SL 40R centrifuge) at a speed of 3000 rpm for 20 min at a temperature of 4°C. The supernatant resulting from the ultracentrifuged process was then appropriately prepared for LC/MS analysis. Equations (1) and (2) were applied to calculate the DL and drug EE, respectively.

$$\text{drug loading efficiency} = \frac{\text{drug precipitate}^{*}}{\text{drug in precipitate} + \text{added excipients}^{**}} \times 100, \tag{1}$$

$$\%\ \text{encapsulation efficiency} = \frac{\text{drug in precipitate}^{*}}{\text{total drug added}} \times 100. \tag{2}$$

*Drug in precipitate = total drug added-free drug after ultracentrifugation. **Added excipients = lipids + surfactants + other ingredients (e.g., in drug nanoformulation).

The simultaneous separation and quantification of PQ, DHA, and LUM in the triple nanoformulated samples were performed using liquid chromatography triple quadrupole mass spectrometer system LC-MS/MS (Agilent technologies 6410-Triple Quadrupole). The mobile phase consisted of (B) 0.5% formic acid in 20 mM aqueous ammonium formate and (C) 0.5% formic acid in acetonitrile. The column used was C-18A, (3 μm PS, 100 × 3.00 mm); infusion concentrations were 100 ng/mL, and the flow rate was 0.3 mL/min. The gradient elution mode used was 0–2.9 min 32% (v/v) (Solvent B) and 68% (v/v) (Solvent C), 3–9 min 28% (v/v) (Solvent B) and 72% (v/v) (Solvent C), and 9–12 min 32% (v/v) (Solvent B) and 68% (v/v) (Solvent C). The total run time was set to 8 min. Detection was performed in multiple reaction monitoring (MRM) mode. Ionization was performed in positive electron spray ionization (+ESI) mode. Nitrogen gas was used as a nebulizing, desolvation, and collision gas (at a pressure of 15.0 psi). The capillary voltage was set to 3500 V, and the gas temperature was set at 300°C. The total scan time was set to 500 ms. The acquisition software was Mass Hunter. The collision energies for PQ, DHA, mefloquine, and LUM were 15.0, 15.0, 30.0, and 35.0 J, respectively.

*3.5. In Vitro Drug Release Studies.* A dissolution experiment was first carried out to determine the appropriate dissolution solution. Briefly, dialysis membrane bags were soaked in the dissolution solution overnight to open up their pores. The in vitro release kinetic study was then conducted by adopting the method used by Gao et al. [47] with slight modifications [47]. The in vitro drug release studies were performed in triplicate.

Twenty milligrams of nanoformulated drug samples was dissolved in 2 mL of 2% (w/v) SLS in 0.1 M acetate buffer (pH 4.5) solution and transferred to the dialysis membrane bags (MWCO: 12–14 kDa). The dialysis membrane bags containing the samples were then placed in a 100-mL beaker filled with 0.1 M acetate buffer (pH 4.5). The beakers were then placed in a shaker incubator operating at 100 rpm and at a temperature of 37°C.

At the start of the experiment, the drug compounds were highly concentrated within the dialysis membrane bags, with zero concentration in the dissolution solution. As the experiment progressed, the concentrated drug solutions diffused from the dialysis membrane bags (regions of high concentration) to the dissolution solution (regions of low concentration) through the dialysis membranes.

Samples (1 mL) of the dissolution solution were periodically collected and replaced with an equal amount of the freshly prepared dissolution solution to maintain the sink condition. The collected samples were further prepared for LC/MS for simultaneous drug quantification using the LC-tandem conditions in Section 3.

*3.6. FTIR Spectroscopy.* FTIR spectroscopy was utilized to characterize and reveal the characteristic functional groups present on the surface of both nanoformulated and free drugs [48]. This technique confirmed the success of the drug encapsulation process. The FTIR spectral analysis was conducted using a (JASCO 4700 ATR-FT/IR) spectrometer. The preparation and analysis of the NPs were performed following a method developed by Thiruvengadam and Bansod [49], with slight modifications.

5.000 mg of the sample was mixed with 95.000 mg of KBr and compressed into a pellet using a press pellet technique. The sample pellet was fixed in the sample cell and placed in the FTIR spectrometer. The FTIR spectrometer was scanned over a spectrum of 4400 to 400 $cm^{-1}$ wavenumber region to obtain spectral readings.

*3.7. Evaluation of Antimalarial Efficacy.* A 4-day Peter's suppressive test was conducted as part of the in vivo antimalarial experiment [50]. The test commenced following approval from the Kenya Medical Research Institute Animal Care and Use Committee (KEMRI ACUC). The research adhered strictly to international guidelines on animal care laboratory use and ethical principles.

Each test group consisted of five Swiss albino mice. These mice were infected intraperitoneally with $1.0 \times 10^7$ parasitized *P. berghei* ANKA RBCs in 0.2 mL inoculum on Day 0. Treatments included six dose levels of DHA–LUM–PQ formulations: free drug without heparin, SLNs without heparin, SLNs functionalized with heparin, free drug with heparin, heparin-functionalized empty NPs, and empty NPs without heparin, administered orally once daily starting 2 hours postinfection. The vehicle used for suspending the samples was administered to the negative control group. Drug administration was repeated at 24, 48, and 72 h postinfection.

On the fourth day postinfection (96 h), peripheral blood films were prepared from the tail snips of each mouse. The blood films were fixed in absolute methanol, stained with 10% Giemsa for 20 min, and examined under a light microscope to estimate parasitemia levels. Chemosuppression percentages (parasite reduction rates) were calculated using the formula described in [51]. All mice used in the in vivo experiments were monitored for a period of sixty days, and survival rates were subsequently computed.

*3.8. Toxicity Studies*

*3.8.1. Ethical Approval.* Acute and subacute toxicity studies were conducted using the Swiss albino mice species. The animal studies were conducted according to the Organization for Economic Cooperation and Development (OECD) guidelines after getting ethical approval from the Institutional Animal Care and Use Committee of Kenya Medical Research Institute. The animals were examined and adapted to the new environmental conditions 7 days prior to the commencement of the experiment.

*3.8.2. Experimental Animals.* Swiss albino mice weighing 18 ± 2 g each of both sexes were provided by the Kenya Medical Research Institute, Animal House. The mice were

maintained under the standard animal house conditions of temperature 25°C ± 2°C, 12-h light–dark cycle, and relative humidity of 75 ± 5%. The mice were fed on mice pellets and tap water ad libitum. The animals were processed according to the standard ethical guidelines for care of laboratory animals throughout the experiment.

*3.8.3. Preparation of the Triple Nanoformulated Drugs for Safety Studies.* The triple nanoformulated drug was prepared using an SLN by adopting the method used in [40, 52]. The drugs and the excipients used were DHA and LUM drugs, surfactants, binders, mucoadhesives, heparin, and SA as the lipid matrix. The resultant drug emulsions were spray-dried using a desktop spray dryer to produce a powder nanoformulated drug. The powdered nanoformulated drugs were dissolved in distilled water and administered to the animals for toxicological evaluations. Distilled water was administered as the negative control to the mice.

*3.8.4. Experimental Design.* Acute and subacute toxicity studies were conducted on the triple nanoformulated drug samples. The studies involved the use of Swiss albino mice.

*3.8.4.1. Acute Toxicity Studies.* The acute toxicity study was conducted as per the up-and-down procedure of OECD guidelines 425 [53]. A limit dose of 2000 mg/kg of the nanoformulated drug was administered to each mouse, and a total of three mice were considered for each sample group. Each mouse was treated with a single oral dose of 2000 mg/kg of the nanoformulated drug in sequence at 48-h intervals. The mice were closely monitored individually at least once during the first 30 min after dosing, periodically during the first 24 h, and daily thereafter, for a total of 14 days for any clinical toxicity sign or mortality. The clinical signs that were being observed on the mice included the skin appearance, the fur texture, eyes, the appearance of the mucous membrane, the effect on the body weight before and after drug administration, and the general behavioral patterns of the mice. The abnormal signs shown by the mice such as salivation, tremors, lethargy, convulsions, diarrhea, sleep, and coma were carefully noted and taken into consideration.

*3.8.4.2. Subacute Toxicity Studies.* The subacute toxicity study on the nanoformulated drug was performed as per the OECD guidelines 407 [54], with slight modifications. Three different drug dosages were selected based on the findings of the drug therapeutic concentrations. The three selected dosages representing the low, middle, and high drug concentrations were considered for the subacute toxicity study.

These low concentration = 257.1 mg/kg, middle concentration = 514.2 mg/kg, and high concentration = 771.3 mg/kg were administered orally daily for 28 days to three different groups of mice ($n = 3$). The last group of mice ($n = 3$) was included as study control and treated the same way with phosphate buffer saline (PBS) solution as the other study samples. After sample treatments, all the experimental mice were daily observed for any abnormal clinical signs and mortality for 28 days of drug administration with the body weights recorded periodically. At the end of the 28-day observation period, the mice were anaesthetized, and their blood samples were collected through cardiac puncture with and without anticoagulant ethylenediaminetetraacetic acid (EDTA), for hematological and biochemical studies, respectively. In hematological studies, white blood cells (WBCs), platelet counts (PLTs), RBC, hemoglobin (HGB), mean corpuscular volume (MCV), mean corpuscular hemoglobin (MCH), and mean corpuscular hemoglobin concentrations (MCHCs) for both control and study samples were determined using a hematology analyzer. For biochemical analysis, blood without any additive was centrifuged at 3000 × $g$ at 4°C for 10 min, serum was separated and alanine aminotransferase (ALT), alkaline phosphatase, aspartate aminotransferase (AST), urea, creatinine (Cr), total bilirubin, direct bilirubin, and indirect bilirubin were estimated using a semiautomated biochemical analyzer. The major body organs such as the liver and the kidney were preserved in 10% buffered formalin for histopathological examinations by standard techniques.

*3.8.4.2.1. Histopathological Studies.* The mice were euthanized and necropsied after the 28$^{th}$ day of the drug administration. Necropsies were keenly conducted on all the mice that were used in the study. The major body tissues such as the liver, kidney, and spleen were carefully removed, weighed, and kept in formalin for further histopathological examination. The relative weight of each organ was computed based on the mice body weights by adopting the formula described in [55]. This is represented in equation (3).

$$\text{relative organ weight} = \frac{\text{organ weight}}{\text{body weight on the day the mice were sacrificed}} \times 100. \quad (3)$$

Histopathological examination was conducted using a standard histopathological technique. Histopathological examination was conducted following a standard histopathological procedure by Mačianskienė [56]. The kidney, liver, and spleen obtained after subtoxicity tests were fixed using 10% neutral buffered formalin solution for 3 h. The fixed tissues were then trimmed to a section thickness of 2 mm and fitted in tissue cassettes and labeled. The cassettes filled with tissues were then stored in formalin.

The fixed tissues were dehydrated by immersing in increasing concentrations of analytical grade 70% ethanol, 90% ethanol, 100% ethanol, and 100% methanol sequentially

for 1, 1.5, 1, and 1 h, respectively, to remove formalin and water. The tissues were then cleared using xylene solution to remove alcohol solvents and embedded using paraffin wax to form a tissue block. The tissue blocks were chilled on ice trays for 10 min before sectioning and sliced into 3-μm ribbons using a microtome. The tissue ribbons were transferred to a warm water bath, allowed to float on the surface, and mounted on microtomy slides. The slides were labeled and placed in a laboratory oven at a temperature of 60°C to deparaffinize and then stained using hematoxylin and eosin stains. The slides were covered by mounting cover slips over the specimen on the slide using optical grade blue to protect it during microscopic examination. The sections were observed at a magnification of X400 (x40-objective lens) under an optical microscope (Optika B-150 Microscope), and the compound microscope (Zeiss Axio scope) was used to capture the histopathological images.

*3.8.4.2.2. Biochemistry Tests.* The blood samples that were collected were centrifuged without any additive at a speed of 4000 rpm for 10 min at a temperature of 4°C and stored at −4°C for further analysis. The blood sample was centrifuged to separate serum from the other blood cells. Blood biochemical analysis was performed using a Erba XL-180 fully automated chemical analyzer. The main indicators of the biochemistry tests include Cr, urea, bilirubin direct (DBIL), AST, and ALT.

*3.8.4.2.3. Hematological Index.* Blood samples for hematological analyses were drawn and placed into EDTA-$K_2$-containing tubes. The hematological test of the mice was conducted at the end of the drug administration period. The hematological parameters were determined using standard biochemistry and hematological tests. Hematological index analysis was performed using a hematology analyzer (Sysmex XS 500i serial number 18403). The following indicators represented the mice hematological index: PLT, MCHC, MCH, MCV, HGB, RBCs, and WBCs.

### *3.9. Quality Control and Data Analysis*

*3.9.1. Quality Control.* The concentrations of antimalarial drugs were determined in blank and double blank samples. Double blank samples consisted of the diluent only 20 Mm ammonium formate: 35% of 0.5% formic acid in acetonitrile (65%:35% [v/v]) while the blank sample consisted of the diluent together with the internal standard (mefloquine) for LC-MS analysis. Internal standard (mefloquine) was used to compensate for any interference/error that might have arisen during sample preparation and analysis. Low-, medium-, and high-quality control points were also considered while constructing standard calibration curves. Each sample was analyzed in triplicate to ascertain the level of accuracy and precision of the analytical technique. For the in vivo experiments, 5 Swiss albino mice were considered per each sample test group and PBS solution was administered to the mice as the negative control for the study. Three Swiss albino mice were considered for each drug concentration for the toxicity study experiments, and PBS was used as a negative control in the toxic study experiments too.

*3.9.2. Data Analysis.* Data were analyzed using statistical methods and software such as Excel, ORIGIN 2018 64Bit, SPSS, Minitab, and M-STAT C. One-way analysis of variance (ANOVA) was used to compare the means of the 11 independent groups considered for the in vivo experiment and the analysis of toxicity data. ANOVA was used to compare the means and determine whether they were statistically significantly different or not. The study data were expressed as mean and standard error means (mean ± SEM). Statistical analyses of hematology, biochemistry, body, and organ weight were performed using ANOVA. A $p < 0.05$ values were considered statistically significant.

## 4. Results and Discussion

*4.1. PSs, Zeta Potential, and PDI of the Triple Nanoformulated Drug.* Experiment 8 resulted in the best NP results in terms of the PS, zeta potential, and PDI as illustrated in Tables 1 and 2. The PSs of the triple nanoformulated drugs were less than 500 nm (< 360 nm). The formed PS was desirable as it has been demonstrated that particles with a diameter of up to 500 nm can easily pass through pores of the gastrointestinal tract (GIT) mucus layer [57]. The smaller size is beneficial to the nanoformulated drugs in terms of swift moving toward the site of infection.

Zeta potential values were greater than 36 mV for NPs without heparin while for those surface modified with heparin, the zeta potential was above −23 mV. Heparin being highly anionic was responsible for transforming the cationic NPs into anionic. Heparin is highly anionic. Our targeted NPs of DHA–LUM–PQ SLNs drug functionalized with heparin had a zeta potential of −35.7 mV.

The modification of NPs with heparin stabilizes them by preventing aggregation, enhancing their biocompatibility, and reducing nonspecific interactions with proteins.

Thus, heparin-induced negative potential has been associated with reduced toxicity due to the negative charge it introduces [58] and enhanced DL and release due to its polyanionic nature particularly for cationic drugs, thus providing a controlled release profile through electrostatic interactions [59].

The negatively charged NPs major advantage includes prolonged circulation time in the bloodstream. This is because they are less likely to interact with plasma proteins and are less readily recognized and cleared by the reticuloendothelial system (RES).

The NP surface properties, such as surface charge, play a critical role in protein adsorption, affecting the drug's biodistribution and pharmacokinetic properties. In the context of drug delivery, surface charge influences how NPs interact with biological systems. Highly cationic NPs tend to be rapidly cleared from the bloodstream due to opsonization and subsequent uptake by the RES [60]. This rapid clearance can limit the effective circulation time of the drug, reducing its therapeutic efficacy.

Table 1: Nanoformulation optimization results.

| Independent variables | | | | Results | | |
|---|---|---|---|---|---|---|
| | | | | Dependent variables | | |
| Experiment number | Homogenizing speed (rpm) | Concentration of chitosan (%) | Homogenizing time (min) | Size (nm) | Zeta potential (mv) | PDI |
| 1 | 3000 | 0.2 | 5 | 293.3 ± 6.525 | −10.2 ± 0.673 | 0.215 ± 0.058 |
| 2 | 8000 | 0.2 | 5 | 308.4 ± 3.837 | −16.0 ± 1.29 | 0.289 ± 0.018 |
| 3 | 3000 | 0.3 | 5 | 590.7 ± 14.18 | −47.7 ± 1.57 | 0.312 ± 0.052 |
| 4 | 8000 | 0.3 | 5 | 551.3 ± 73.29 | −17.5 ± 2.03 | 0.850 ± 0.130 |
| 5 | 3000 | 0.2 | 15 | 549.2 ± 136.3 | −31.10 ± 2.19 | 0.835 ± 0.094 |
| 6 | 8000 | 0.2 | 15 | 276.5 ± 4.38 | −27.0 ± 4.38 | 0.380 ± 0.078 |
| 7 | 3000 | 0.3 | 15 | 576.6 ± 87.21 | −30.3 ± 2.45 | 0.74 ± 0.05 |
| 8 | 8000 | 0.3 | 15 | 357.1 ± 57.14 | −35.7 ± 1.25 | 0.657 ± 0.091 |

Table 2: The particle sizes, polydispersity index values, and zeta potential of empty and triple nanoformulated drugs.

| S. nos. | Sample | Particle size (nm) | Zeta potential (mV) | Polydispersity index |
|---|---|---|---|---|
| 1 | Empty nanoparticle without heparin | 286.0 ± 14.03 | 36.5 ± 1.04 | 0.477 ± 0.042 |
| 2 | Empty nanoparticle with heparin | 265.6 ± 10.02 | −23.8 ± 3.3 | 0.410 ± 0.94 |
| 3 | DHA–LUM–PQ SLNs drug functionalized without heparin | 277.6 ± 30.41 | 48.1 ± 1.35 | 0.366 ± 0.150 |
| 4 | DHA–LUM–PQ SLNs drug functionalized with heparin | 357.1 ± 57.14 | −35.7 ± 1.25 | 0.657 ± 0.091 |

*4.2. Stability Study Results of the Triple Nanoformulated Drugs.* Figures 1 and 2 show the summarized stability study results for triple nanoformulated drugs. The drugs were stored at varied temperature conditions for ninety days. The 90-day storage of the triple nanoformulated drugs did not show any significant changes in the particle charges, size, and homogeneousness. A study conducted by Marante et al. 2020 on the effect of spray-drying on polymeric nanoformulations indicated that spray-drying improves the long-term stability of the NPs [61]. Therefore, the stability of the NPs in terms of size, homogeneity, and charges could be attributed to the fact that the drug emulsions were dried through a spray-drying process. Results that are comparable to these were reported in earlier studies that involved the nanoformulation of DHA into lipid structure nanocarrier and its suspensions [40, 62].

*4.3. In Vitro Drug Release Kinetic Results.* The drug release kinetic studies were carried out for a period of seventy-two hours, and the summary results are reported in Table 3 and Figures 3, 4, 5, 6, 7, and 8. The drug release data obtained were analyzed using different pharmaceutical models such as zero-order kinetics, Higuchi, first-order kinetics, Korsmeyer–Peppas, and Hixson Crowell as proposed by Dash et al. (2010) [63]. The best-fitted model with the release data is assessed by the coefficient of determination ($R^2$) value [64]. The higher $R^2$ values show the best line of fit, hence the model describing the release profile of the drug. $R^2$ values were computed from the plots of log cumulative % drug release versus time for the Korsmeyer–Peppas model, cumulative drug release versus time for zero order, and cumulative drug release versus square root of time for the Higuchi model. The plot for the first-order model was performed by plotting log cumulative % of drug remaining versus time while the $R^2$ value of the Hixson–Crowell model was calculated by using a plot of (cubic root of the total amount of drug (%)–cubic root of drug remaining (%) versus time). The computed $R^2$ values are recorded in Table 3.

PQ, DHA, and LUM drugs followed the Korsmeyer–Peppas drug release model as shown in Figures 3, 4, and 5. The three drugs also followed the Higuchi model as shown in Figures 6, 7, and 8. Higuchi drug release model is a diffusion-controlled release [65]. In this case, the free drugs moved from the visking tubing containing highly concentrated drugs to the dissolution solutions with zero drug concentrations at time, $t = 0$ s through the process of diffusion. The Kosmeyer–Peppas model has been successfully applied in the liposomal doxorubicin formulations for drug-gene delivery [66]. Higuchi and Korsmeyer–Peppas drug release models have also successfully explained the drug release kinetics of extended-release levodopa and carbidopa tablets [65]. The three drugs (DHA–LUM–PQ) in the triple nanoformulated drugs considered in this experiment were effectively described by Higuchi and Korsmeyer–Peppas drug release models. A burst drug release was shown by DHA, PQ, and LUM drugs in the first six hours followed by drug-controlled release over the remaining hours. The drug release curves flattened after the 24$^{th}$ hour of the drug release, and this showed that the drug concentrations in the dissolution solution levelized that within the visking tubing bag, an indication that the concentration gradient was attained.

*4.4. DL and EE.* The DL capacities of DHA, PQ, and LUM in the triple nanoformulated drugs were 11.87 ± 0.04%, 8.01 ± 0.09%, and 24.10 ± 2.88%, respectively. The EE results of DHA, PQ, and LUM in the triple nanoformulated drugs were 93.98 ± 0.41%, 87.60 ± 0.64%, and 42.03 ± 9.46%, respectively. These results are similar to the previous studies conducted on drug nanoformulation using SLNs as a drug carrier. A previous study conducted in [67] on the use of SLNs for the controlled delivery of poorly water-soluble nonsteroidal anti-inflammatory steroid drugs reported entrapment efficiencies ranging between 52% and 68% and DL percentages of 2.4%–6.9% [67]. A study conducted by Farzaneh et al. in 2020 on the preparation, optimization, and characterization of a-tocopherol-loaded SLNs reported entrapment efficiency values of 87.47 ± 2.41%, 90.85 ± 1.30%, and 74.32 ± 1.64% for the drug different concentrations. The DL efficiencies of 42.46 ± 1.17%, 59.38 ± 0.84%, and 54.92 ± 1.21% were also reported [68]. The drug encapsulation as a process of NP preparation involves a drug coloading process. SLNs are an example of a drug coloading strategy [69].

*4.5. FTIR Spectra of Triple Nanoformulated DHA–LUM–PQ Drug.* FTIR overlay spectra of the empty NP, free, and nanoformulated drugs are shown in Figure 9. The FTIR bands of the empty NPs and triple nanoformulated drugs exhibited almost the same absorption peaks. The wavenumbers exhibited in both the empty and triple nanoformulated drugs represent the functional groups of the compounds that make up the nanoformulation excipients. These included the mucoadhesive chitosan, SA which acted as the matrix, and the PVA which was applied as a surfactant. The wavenumbers that were displayed in both the empty and the triple nanoformulated drug samples were the absorption peaks that represented the presence of PVA showed an absorption peak of 3308.29 $cm^{-1}$ showing the

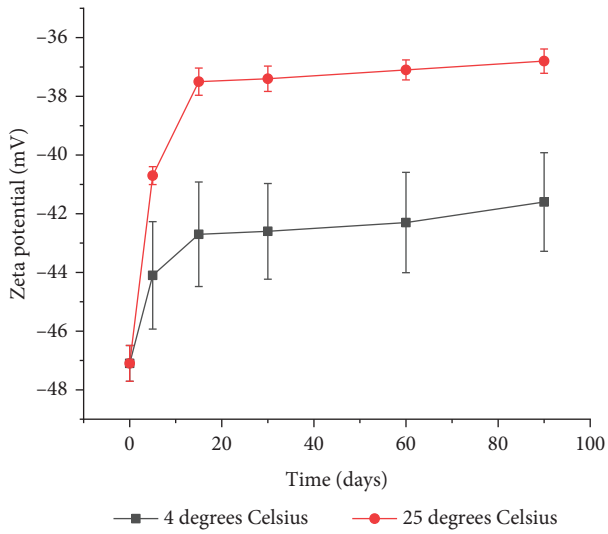


Figure 1: Nanoparticle zeta potential variations with changes in temperature.

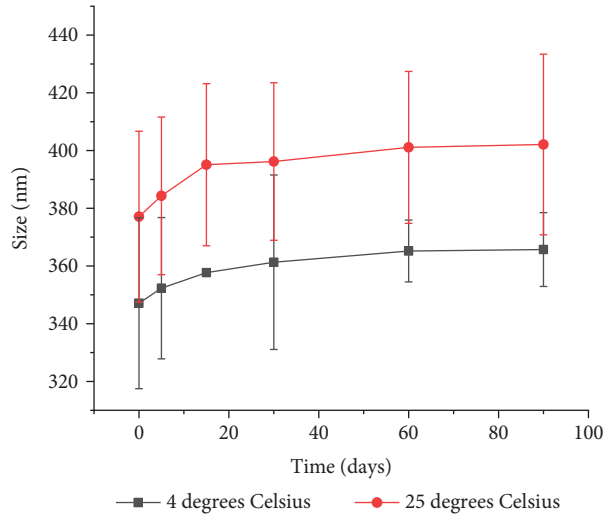


Figure 2: Nanoparticle size variations with changes in temperature.

Table 3: $R^2$ values of the lines produced by the DHA, PQ, and LUM release profile data analyzed using varied pharmaceutical models.

| S. nos. | Drug release kinetic model | PQ $R^2$ value | DHA $R^2$ value | LUM $R^2$ value |
|---|---|---|---|---|
| 1 | Korsmeyer–Peppas | 0.9650 | 0.9535 | 0.9728 |
| 2 | Higuchi | 0.9167 | 0.9102 | 0.9237 |
| 3 | First order | 0.7877 | 0.7685 | 0.8333 |
| 4 | Hixson | 0.7740 | 0.7504 | 0.8240 |
| 5 | Zero order | 0.7467 | 0.7138 | 0.8057 |

presence of -OH in the structure of PVA. An absorption peak at 2914.88 $cm^{-1}$ signified a strong band that is related to C-H in PVA [70]. The absorption peak at 2853.17 $cm^{-1}$ represented an aliphatic C-H vibration in SA [71], the absorption peak at 1416.46 $cm^{-1}$ represented C-O bending peak in SA while the absorption peak found at around

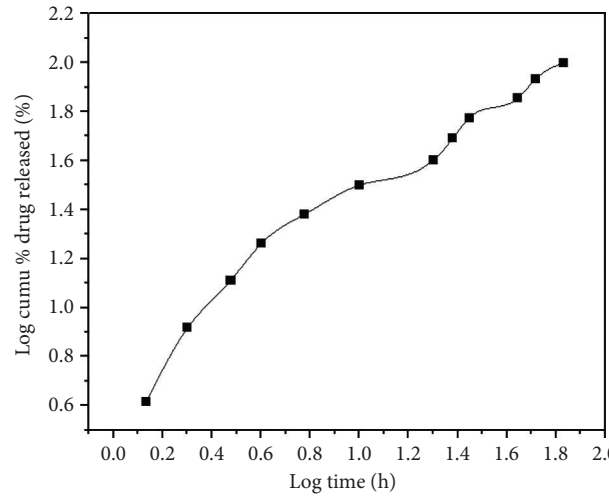


Figure 3: Kors–Peppas mathematical model followed by primaquine drug in the triple nanoformulated samples.

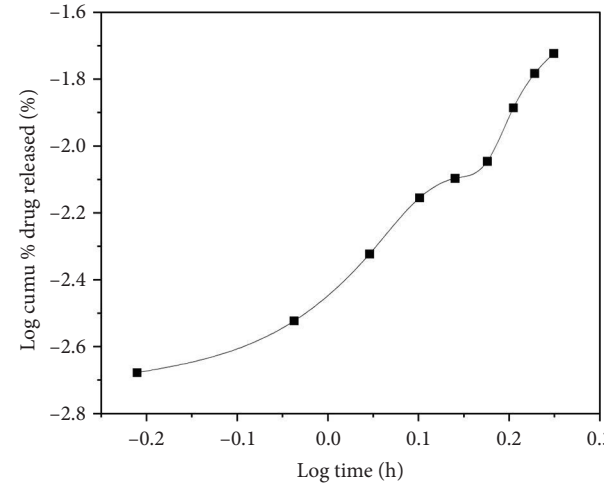


Figure 4: Kors–Peppas mathematical model followed by dihydroartemisinin drug in the triple nanoformulated samples.

1372.10 $cm^{-1}$ represented the $CH_3$ symmetrical deformations in chitosan [72]. The bending vibrations hydroxyls existing in chitosan molecules were represented by the absorption peaks that were found at around 1248.68 $cm^{-1}$ as reported in [73]. The FTIR overlay spectra showed that the triple nanoformulated drug had less pronounced peaks than the three free drugs. The OH- absorption peak that was more pronounced in the DHA-free drug samples at wavelength number 3732 $cm^{-1}$ was not present in the triple nanoformulated drug samples. On the other hand, LUM-free drug displayed pronounced absorption peaks at C-O stretching at 1139.22 $cm^{-1}$, O-H aromatic stretching at 3402.70 $cm^{-1}$, and C=C aromatic stretching at 1575.43 $cm^{-1}$; the pronounced peaks that were exhibited in the LUM-free drugs were absent in the triple nanoformulated drug. PQ-free drugs also displayed pronounced absorption peaks at $NH_2$ bending at 1586.17 $cm^{-1}$ and C=C stretching bonds at around 1532 and 1458.89 $cm^{-1}$,

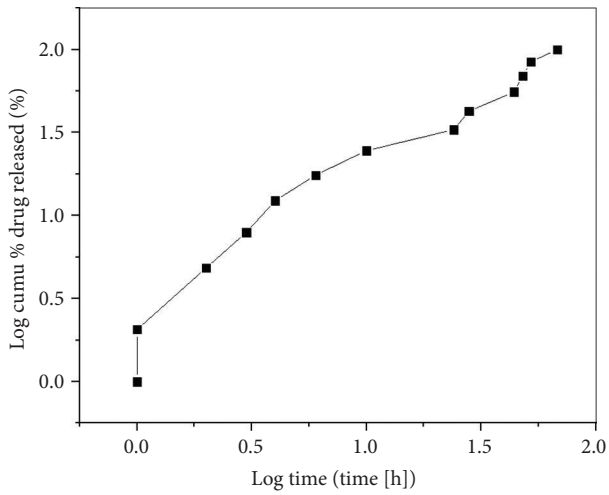


Figure 5: Kors–Peppas mathematical model followed by lumefantrine drug in the triple nanoformulated samples.

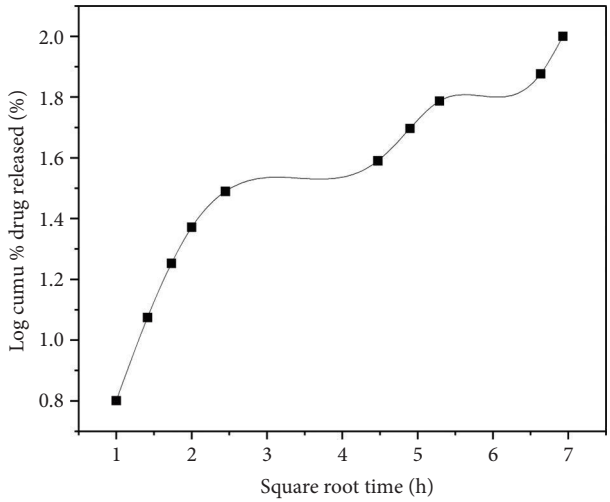


Figure 6: Higuchi mathematical model followed by dihydroartemisinin drug in the triple nanoformulated samples.

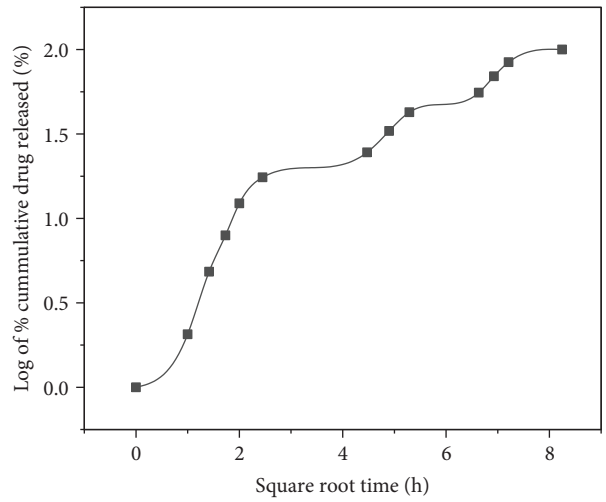


Figure 7: Higuchi mathematical model followed by lumefantrine drug in the triple nanoformulated samples.

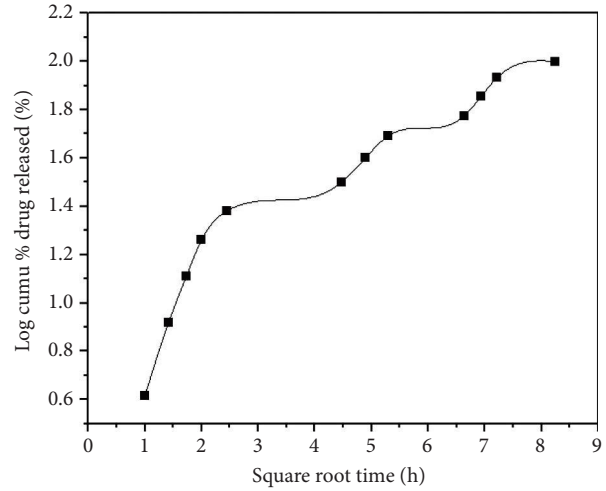


Figure 8: Higuchi mathematical model followed by primaquine drug in the triple nanoformulated samples.

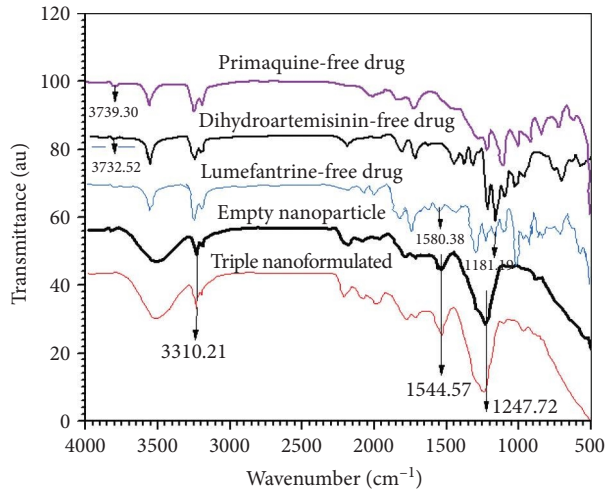


Figure 9: FTIR overlay spectra for empty nanoparticles, free drugs (DHA, PQ, and LUM) and triple nanoformulated drugs.

which were absent in the triple nanoformulated drug. This was an indication of a successful drug encapsulation process, where the drug-APIs were successfully enclosed within the SLN core. DLM which acted as a structure binder in the nanoformulation process could have contributed to this by further reducing the number of pronounced peaks in the triple nanoformulated drugs. [46].

*4.6. Morphological Analysis.* The images of the DHA–PQ–LUM triple nanoformulated drugs from the SEM are shown in Figure 10. The triple nanoformulated drugs captured by SEM equipment display sphere-shaped images whose surfaces are fibrous and smooth. The sphere-based shapes and smooth images were associated with the SLN, the main nanocarrier used in the nanoformulation process [74]; the chitosan used as a mucoadhesive in the nanoformulation process has fibrous surfaces that are aimed at improving the drugs' biodegradability and biocompatibility [75]. This

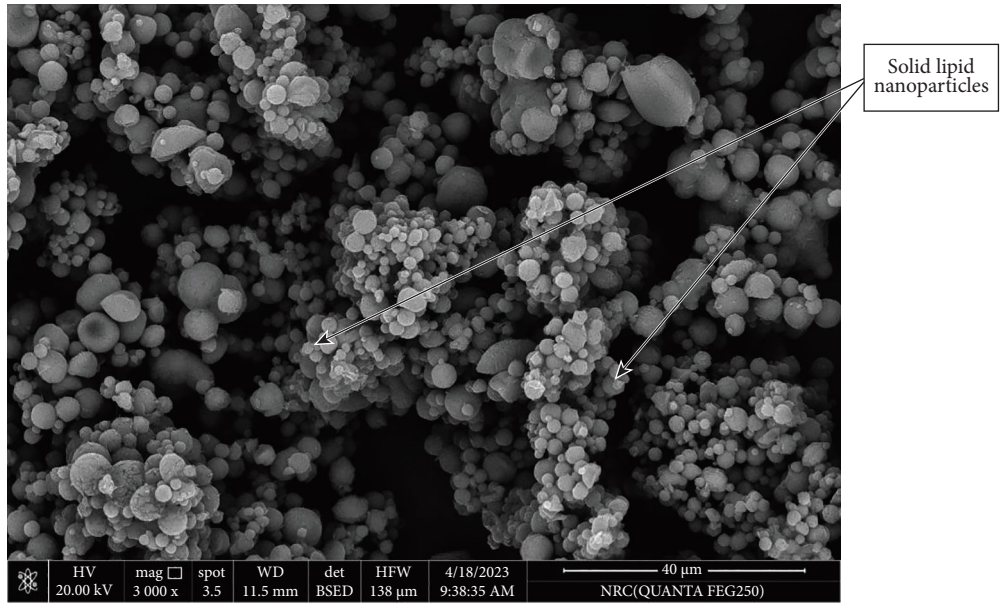


Figure 10: SEM images for the solid lipid triple nanoformulated drug.

could have potentially contributed to the fibrous surface of the resultant triple nanoformulated drug. The SEM image further exhibited moderately homogeneous granulated particles that were interwoven to each other with pores existing between them. A study in [76] showed that particles that are granulated and homogeneous and have porous structures are greatly important in biological applications. Therefore, the resultant triple nanoformulated drug could potentially show great antimalarial efficacy.

The SEM image (Figures 10 and 11) shows spherical nanoformulated drug particles having embedded fibers on their surfaces. The spherical particles are the SLNs used as the nanocarriers in the nanoformulation process [74]. The embedded fibers are attributed to chitosan used as a mucoadhesive in the nanoformulation process which are fibrous in nature. Chitosan is used to improve the drugs' biodegradability and biocompatibility [75].

The SEM images (Figure 12) further exhibited nanoformulated drug particles with porous surfaces. A study conducted by Rahman et al. [76] showed that homogeneous and porous structures are important in biological applications. The porous structures have unique properties such as tunable shapes and pore size, large surface area-to-volume ration, and tunable density that enable it to bind with a large number of functional groups within its pores, hence exhibiting great biological activity. Therefore, the resultant triple nanoformulated drug could potentially show great antimalarial efficacy.

*4.7. Antiplasmodium Efficacy.* In vivo experiments were conducted using female Swiss albino mice to examine the antiplasmodium efficacy. The results, shown in Table 4, involved six test groups: DHA–LUM–PQ-free drugs with heparin, DHA–LUM–PQ-free drugs without heparin, triple nanoformulated drugs, empty NPs functionalized with heparin, empty NPs without heparin, and distilled water as the negative control. The use of empty NPs allowed for the assessment of the effects of nanoformulation excipients on plasmodium parasites.

The test groups treated with the negative control and empty NPs without heparin displayed the least chemosuppression percentages, indicating minimal to no antimalarial activity. In contrast, the empty NPs functionalized with heparin showed comparatively higher chemosuppression percentages. This increased efficacy can be attributed to heparin's role as a glycosaminoglycan, which has a high affinity for pRBCs [49]. Heparin's antimalarial properties have been noted in other studies as well, where it was shown to disrupt merozoite invasion and reduce parasitemia levels [77].

The triple nanoformulated drugs demonstrated significantly higher parasite chemosuppression efficiency compared to the free-drug counterparts. This enhanced efficacy is consistent with findings from previous research on nanoformulated antimalarial drugs. For instance, nanoformulation of artemether–LUM using nanostructured lipid carriers for oral malaria therapy resulted in improved antimalarial activity and better pharmacokinetic profiles compared to nonformulated drugs [78]. Similarly, studies on the nanoformulation of PQ and DHA using SLNs as carriers have reported enhanced drug efficacy and reduced toxicity [40, 46].

None of the mice treated with the triple nanoformulated drugs died during the 60 days of monitoring, resulting in a 100% survival rate. Conversely, the mice treated with free drugs had significantly lower survival rates of $41.33 \pm 3.65\%$ and $37.33 \pm 5.81\%$ for those without and with heparin, respectively. The free-drug-treated mice also displayed toxicity signs such as general body weakness, diarrhea, and rough fur, highlighting the benefits of nanoformulation in reducing drug toxicity.

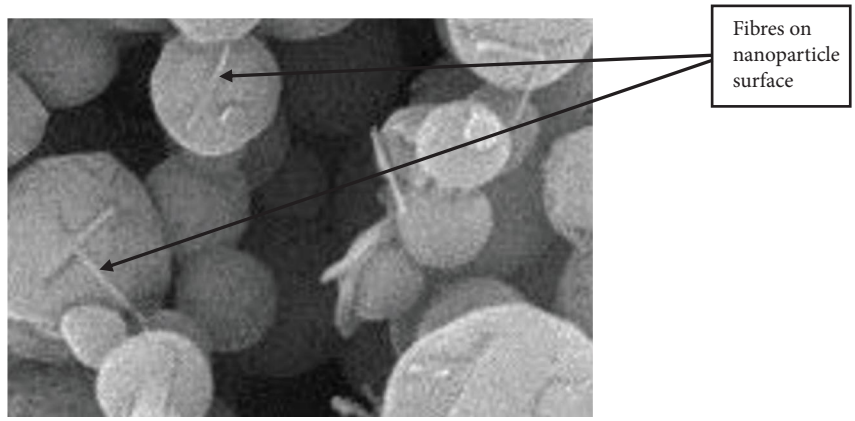


Figure 11: SEM image (zoomed in) showing fibers embedded on the surface of the spherical nanoparticles.

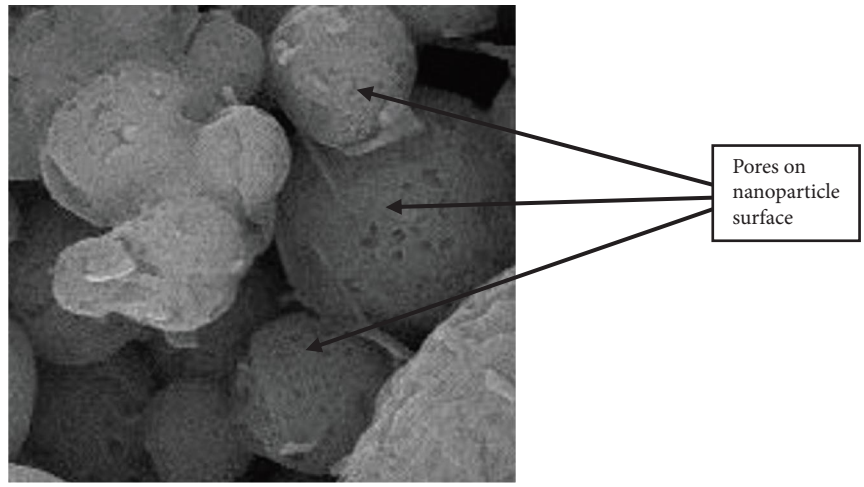


Figure 12: SEM image (zoomed in) showing pores on the surface of the spherical nanoparticles.

Table 4: Percentage chemosuppression efficiency of test group samples in the suppressive test against *Plasmodium berghei aNKa* test and mice survival rates.

| S. nos. | Drug sample | Average% chemosuppression efficiency mean ± std | Survival rates (%) |
|---|---|---|---|
| 1 | Triple nanoformulated drug with heparin | 91.37 ± 4.25 | 100.00 ± 00 |
| 2 | Triple nanoformulated drug without heparin | 71.44 ± 10.05 | 100.00 ± 00 |
| 3 | DHA–LUM–PQ-free drugs with heparin | 61.82 ± 8.27 | 77.33 ± 5.81 |
| 4 | DHA–LUM–PQ-free drugs without heparin | 59.15 ± 8.92 | 71.13 ± 3.65 |
| 5 | Empty nanoparticle with heparin | 24.12 ± 7.13 | 38.00 ± 7.16 |
| 6 | Empty nanoparticle without heparin | 0.00 ± 0.00 | 0.00 ± 0.00 |
| 7 | Negative control | 0.00 ± 0.00 | 0.00 ± 0.00 |

The significant difference in chemosuppression efficiency ($p < 0.05$) between the triple nanoformulated drugs and free drugs aligns with findings from various studies that have demonstrated the advantages of nanoformulated drugs in enhancing antimalarial efficacy. For example, NPs have been shown to improve drug solubility, stability, and bioavailability, leading to better therapeutic outcomes [79].

The in vivo experiments underscore the superior antimalarial efficacy of triple nanoformulated drugs over free-drug counterparts, corroborating previous research on the benefits of nanoformulation in malaria therapy. The inclusion of heparin as a functionalizing agent further enhances the chemosuppression potential due to its specific affinity for pRBCs, providing a promising approach to improving the effectiveness and safety of antimalarial treatments.

In summary, the nanoformulation of multiple antimalarial drugs into a single unit, as demonstrated with the DHA–LUM–PQ–heparin combination, represents a significant advancement in malaria treatment. This approach simplifies dosing regimens, enhances bioavailability, and targets drug delivery.

### 4.8. Safety Study

*4.8.1. Acute Toxicity Study.* No toxic symptom was observed in the mice in the acute toxicity study. The toxic symptoms that were being monitored included rough hair, depression, diarrhea, restlessness/dizziness, and the major body tissues including the liver, spleen, and kidney were observed for any abnormal sign in terms of color change, change in size, and bleeding spots. The number of mortalities was also recorded during the 14 days of drug administration. The major body tissues did not show any sign of abnormality, and no mortalities were recorded throughout the 14 days of drug administration. The experimental mice showed a normal increase in body weight as shown in Table 5. This shows that the drugs administered at a concentration of 2000 mg/kg did not have any adverse effects on the mice weights.

A drug concentration of 2000 mg/kg was used in the acute toxicity study representing the drug dosage that Globally Harmonized System (GHS) of classification and labeling of chemicals considers safe for the rodents [80]. The lethal dose $(LD)_{50}$ of the triple nanoformulated drug was 2,000 mg/kg because no mortalities or toxicity signs were observed during the 14 days of the acute toxicity study. The drug was therefore considered safe according to the GHS standards [80].

*4.8.2. Subacute Toxicity.* In the subacute toxicity study, the study mice did not show any visual sign of toxicity, and no mortalities were recorded during the 28 days of drug administration and mice monitoring as illustrated in Table 6. Figure 13, on the other hand, shows normal variations in the mice weights recorded for the entire study period. Monitoring the body weight changes during toxicity study is a key indicator of adverse effects of chemical and pharmaceutical compounds [81, 82]. Table 7 shows the descriptive statistics and the $p$ values of the relative organ weights, and biochemical and hematological parameters. $p$ values < 0.05 show that the values are significantly different from the control, and therefore, a possible indication of toxicity and $p$ values > 0.05 show otherwise. The detailed statistical analysis data are represented in Table 7. The $p$ values for all the parameters were greater than 0.05. This shows that the triple nanoformulated drug was safe for the experimental Swiss albino mice.

The blood hematological analysis greatly predicts drug risk assessment since the hematopoietic system is among the sensitive markers for toxic compounds [82]. The hematological parameters for the medium concentration of the triple nanoformulated drugs did not show any significant difference as compared to the control sample. This was an indication that the triple nanoformulated drug used at different concentrations was safe for the experimental mice. The kidney function markers such as urea, albumin, and Cr did not show any significant difference in comparison to the control sample, hence showing that the drug administered at three different concentrations did not have any antagonistic effect on the kidney. The biochemical parameters such as AST, ALT, and DBIL, which are liver biomarkers did not show any significant difference, hence an indication that the administered drugs did not have any adverse effects to the liver functions. Overall, the drug mainly targets the liver where drug metabolism takes place and thereafter expelled through the hepatobiliary system.

The organ images of the liver and spleen of the treated mice did not show any physical variation from the organs of the negative control as shown in Figure 14.

This shows that the triple nanoformulated drug was safe for the experimental Swiss albino mice.

Table 5: Mice weight variations in acute toxicity study.

| | Day 0 | Day 7 | Day 14 |
|---|---|---|---|
| Drug concentration (2000 mg/kg) b.w | 24.25 ± 2.22 | 24.75 ± 2.87 | 25.00 ± 2.83 |

Table 6: Mice mortality rates during the acute toxicity study.

| Group | Dosage (mg/kg) | No. dosed | Survival rates (%) |
|---|---|---|---|
| *DHA and LUM&PQ* | | | |
| DLP1 | 257.1 | 3 | 100 |
| DLP2 | 514.2 | 3 | 100 |
| DLP3 | 771.3 | 3 | 100 |
| Negative control (distilled water) | 0 | 5 | 100 |

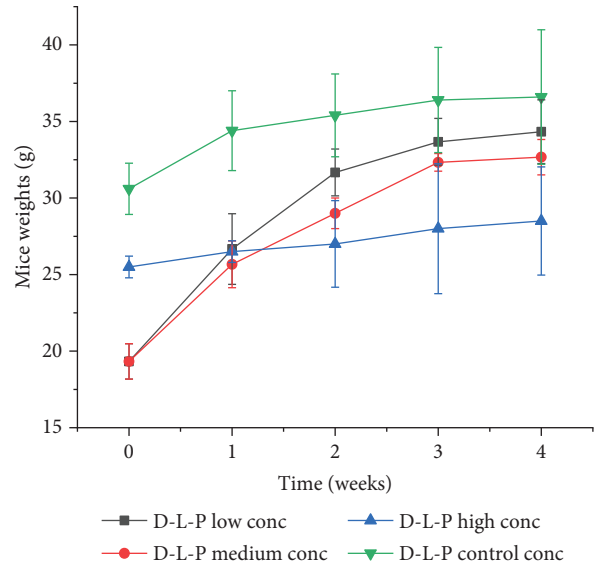


Figure 13: Line graph showing weight variations of mice during subacute toxicity study.

Table 7: $p$ values and statistical data analysis for relative organ weights, hematological, and biochemical parameters.

| Parameters | Normal control | Low concentration (257.1 mg/kg) | Medium concentration (514.2 mg/kg) | High concentration (771.3 mg/kg) | $p$ value |
|---|---|---|---|---|---|
| *Organ relative weights* | | | | | |
| Spleen | 0.601 ± 0.084 | 0.505 ± 0.058 | 0.562 ± 0.045 | 0.577 ± 0.032 | 0.695 |
| Kidney | 2.323 ± 0.156 | 2.383 ± 0.071 | 2.549 ± 0.147 | 2.101 ± 0.094 | 0.155 |
| Liver | 7.195 ± 0.318 | 7.368 ± 0.255 | 7.535 ± 0.337 | 7.884 ± 0.113 | 0.376 |
| *Hematological parameters* | | | | | |
| White blood cells ($\times 10^3$ u/L) | 4.39 ± 0.16 | 3.69 ± 0.35 | 5.40 ± 0.78 | 4.13 ± 0.11 | 0.112 |
| Red blood cells ($\times 10^6$ u/L) | 10.69 ± 0.35 | 9.91 ± 0.80 | 10.81 ± 0.22 | 10.94 ± 0.42 | 0.497 |
| HGB (g/dL) | 15.90 ± 0.55 | 14.73 ± 0.98 | 15.77 ± 0.48 | 13.97 ± 0.45 | 0.197 |
| HCT (%) | 54.73 ± 0.12 | 51.23 ± 2.34 | 54.97 ± 1.42 | 45.03 ± 2.47 | 0.017 |
| Mean corpuscular volume (fL) | 49.30 ± 0.21 | 50.23 ± 1.27 | 50.83 ± 0.70 | 45.43 ± 1.89 | 0.048 |
| Mean corpuscular hemoglobin concentration | 30.17 ± 0.13 | 28.90 ± 0.60 | 28.67 ± 0.52 | 29.73 ± 0.39 | 0.137 |
| Platelets ($\times 10^3$ UL) | 975.70 ± 18.20 | 862.30 ± 33.60 | 922.70 ± 21.80 | 942.00 ± 29.60 | 0.083 |
| *Biochemical parameters* | | | | | |
| ALT/GPT (U/L) | 54.40 ± 2.14 | 57.43 ± 2.11 | 56.23 ± 2.01 | 56.53 ± 2.62 | 0.807 |
| AST/GOT (U/L) | 183.63 ± 4.06 | 187.23 ± 5.97 | 181.47 ± 4.21 | 183.33 ± 3.67 | 0.839 |
| Bilirubin direct (mg/dL) | 0.080 ± 0.010 | 0.073 ± 0.009 | 0.083 ± 0.015 | 0.067 ± 0.009 | 0.713 |
| Urea | 50.07 ± 0.88 | 51.10 ± 1.69 | 50.17 ± 0.30 | 50.00 ± 1.14 | 0.885 |
| Creatinine | 0.50 ± 0.01 | 0.51 ± 0.03 | 0.50 ± 0.03 | 0.46 ± 0.032 | 0.461 |

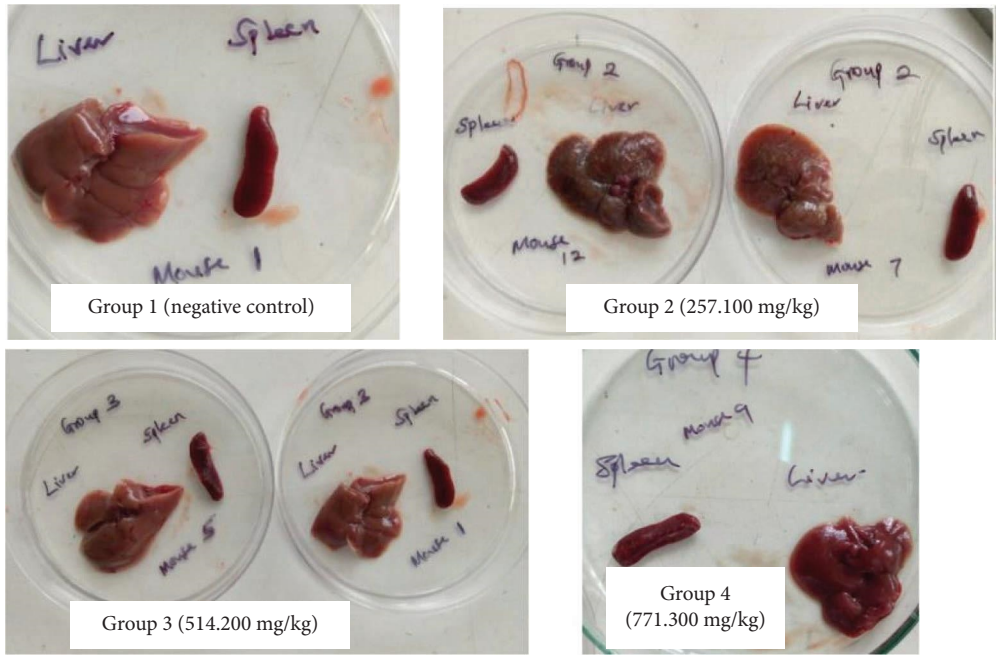


FIGURE 14: The images of Swiss albino mice liver and spleen of representative mice treated with distilled water and triple nanoformulated drugs.

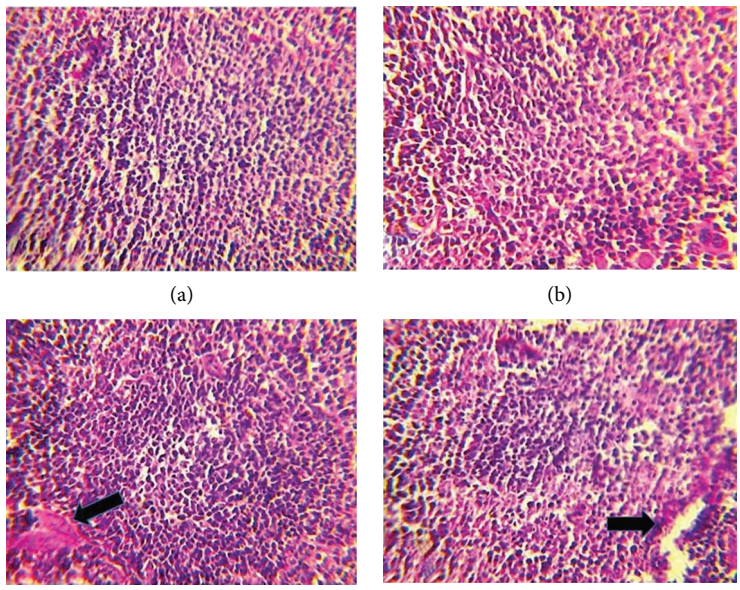


FIGURE 15: Histopathological image of Swiss albino mice spleen—arrow sequestration of splenocytes. (a) Normal control (distilled water), (b) low drug concentration (257.1 mg kg), (c) medium drug concentration (514.2 mg kg), and (d) high blood concentration (771.3 mg kg).

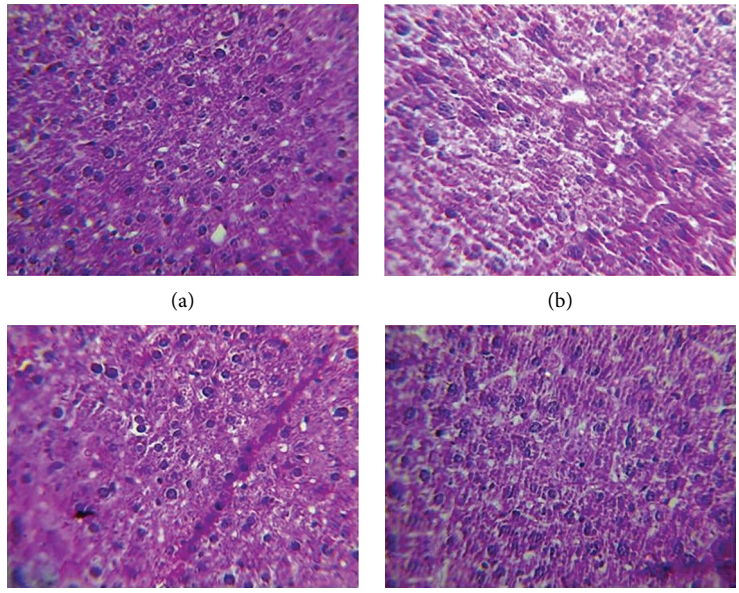


FIGURE 16: Histopathological image of Swiss albino mice liver. (a) Normal control (distilled water), (b) low drug concentration (257.1 mg/kg), (c) medium drug concentration (514.2 mg/kg), and (d) high blood concentration (771.3 mg/kg).

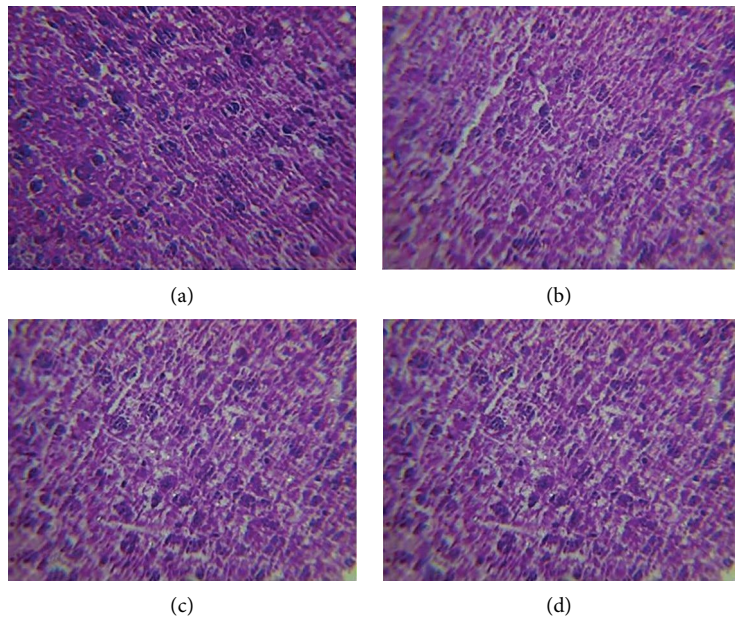


FIGURE 17: Histopathological image of Swiss albino mice kidney. (a) Normal control (distilled water), (b) low drug concentration (257.1 mg/kg), (c) medium drug concentration (514.2 mg/kg), and (d) high blood concentration (771.3 mg/kg).

The histopathological images of the liver, spleen, and kidney of the treated mice did not show any variation from the organs of the negative control as shown in Figures 15, 16, and 17. The liver and kidney tissues (Figures 14 and 18) for the treated mice with the triple nanoformulated drug were normal. The spleen tissues showed sequestration of splenocytes (shown by the arrows) in drug samples of middle and high concentrations (Figure 15). This is an indication

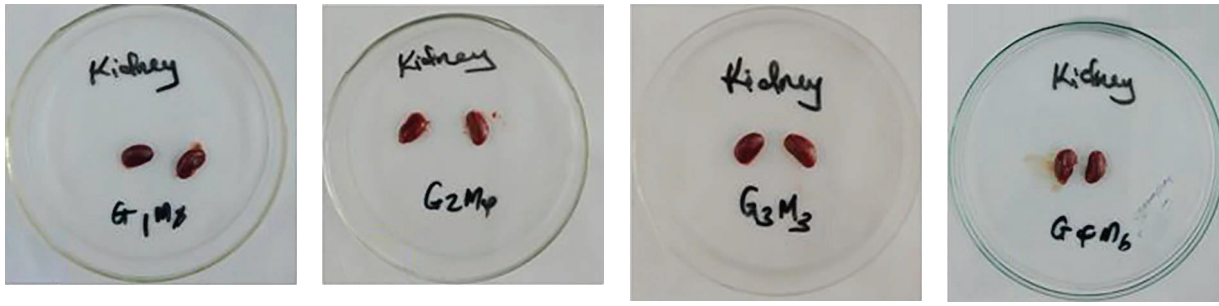


(a) (b) (c) (d)

FIGURE 18: The images of Swiss albino mice kidney of representative mice treated with distilled water (a), triple nanoformulated drugs (b) 257.100 mg kg, (c) 514.200 mg kg, and (d) 771.300 mg kg.

that the spleen tissues were reacting to the presence of a foreign substance in the blood attributed to the triple nanoformulated drug. This is a normal response of the spleen to foreign substances in the blood [83].

## 5. Conclusion

The triple nanoformulated drug was successfully prepared using a solid lipid nanocarrier and spray-dried using a bench-top spray-dryer. The triple nanoformulated drugs had PSs < 500.00 nm. The zeta potentials of the triple nanoformulated drugs were greater than −30.00 mV representing stable nanoformulated drugs while the PDI values obtained were less than 0.70 indicating a homogeneous drug. SEM images showed spherical nanoformulated drug particles having embedded fibers on their surfaces. The spherical particles which consisted of SLNs were used as the nanocarriers in nanoformulation process. The SEM images further exhibited nanoformulated drug particles with porous surfaces which improves the biological activity of the drug. The FTIR bands of the empty NPs and triple nanoformulated drugs exhibited similar absorption peaks. The absorption peaks (C-H, -OH, and C-O) in both the empty and triple nanoformulated drugs are due to functional groups of the compounds that make up the nanoformulation excipients. These included the mucoadhesive chitosan, SA matrix, and the PVA surfactant. The FTIR overlay spectra showed that the triple nanoformulated drug had less pronounced peaks than the free drugs. These observations of absent peaks when the drugs were used in the nanoformulation process indicated a successful drug encapsulation process, where the drug APIs were successfully enclosed within the SLN core. The DL capacities for DHA, LUM, and PQ were 11.87%, 24.10%, and 8.01%, respectively, while the EEs for DHA, LUM, and PQ were 93.98%, 42.03%, and 87.60%, respectively. Drug EE and loading capacity were determined, and this was an indication of a successful drug nanoformulation process. Kors–Peppas and Higuchi models best described the drug release kinetics for DHA, LUM, and PQ. The storage temperature conditions of 4°C and 25°C did not significantly affect the sizes and zeta potentials of the triple nanoformulated drugs stored over a period of 90 days indicating a stable drug formulation. The DHA–LUM–PQ triple nanoformulated drug was 30% more efficacious compared to conventional oral dose. DHA–LUM–PQ-free drugs were tested in the Swiss albino mice infected with *Plasmodium berghei* ANKA malaria parasites. This is attributed to the controlled release of the drug between 7–68 h of drug release. The acute and subacute studies of the triple nanoformulated drugs conducted on the Swiss albino mice showed that the triple nanoformulated drug was safe and did not affect the mice body weights, liver, kidney, and spleen, and no mice mortalities were recorded during the 14 and 28 days of acute and subacute toxicity studies, respectively. This research demonstrated that a nanomedicine delivery system of triple combined antimalarial drug was successfully developed and tested.

## Data Availability Statement

The data are available in supporting information.

## Conflicts of Interest

The authors declare no conflicts of interest.

## Funding

This work was supported by the Kenya National Research Fund (grant number NRF/1/114).

## Acknowledgments

The authors of this study sincerely thank the National Research Fund (NRF), Kenya, for funding this work. The authors would also wish to express their gratitude to the Kenya Medical Research Institute (KEMRI), The Centre for Research in Therapeutic Sciences (CREATES)-Strathmore University, The Technical University of Kenya (TUK), and the Kenya Institute of Primate Research (KIPRE) for availing the essential facilities to conduct the research study and creating a conducive environment for the research work.

## References

[1] World malaria report, "World Malaria Report 2022" (2022).
[2] M. Al-Awadhi, S. Ahmad, and J. Iqbal, "Current Status and the Epidemiology of Malaria in the Middle East Region and

beyond," *Microorganisms* 9, no. 2 (2021): 338–420, https://doi.org/10.3390/microorganisms9020338.

[3] D. Shi, L. Wei, H. Liang, D. Yan, J. Zhang, and Z. Wang, "Trends of the Global, Regional and National Incidence, Mortality, and Disability-Adjusted Life Years of Malaria, 1990–2019: An Analysis of the Global Burden of Disease Study 2019," *Risk Management and Healthcare Policy* 16 (2023): 1187–1201, https://doi.org/10.2147/RMHP.S419616.

[4] P. Tindana, F. de Haan, C. Amaratunga, et al., "Deploying Triple Artemisinin-Based Combination Therapy (TACT) for Malaria Treatment in Africa: Ethical and Practical Considerations," *Malaria Journal* 20, no. 1 (2021): 119–127, https://doi.org/10.1186/s12936-021-03649-7.

[5] S. A. Ayinbuomwan, A. O. Opadeyi, and A. O. Isah, "The Current Use of the Artemisinin-Based Combination Therapies in Adult Patients at a Tertiary Hospital, South-South Nigeria," *Babcock University Medical Journal* 5, no. 2 (2022): 68–77, https://doi.org/10.38029/babcockunivmedj.v5i2.145.

[6] B. R. Adegbite, J. R. Edoa, Y. J. Honkpehedji, et al., "Monitoring of Efficacy, Tolerability and Safety of Artemether-Lumefantrine and Artesunate-Amodiaquine for the Treatment of Uncomplicated Plasmodium Falciparum Malaria in Lambaréné, Gabon: An Open-Label Clinical Trial," *Malaria Journal* 18, no. 1 (2019): 1–9, https://doi.org/10.1186/s12936-019-3015-4.

[7] D. M. Rathod, K. R. Patel, H. N. Mistri, A. G. Jangid, P. S. Shrivastav, and M. Sanyal, "Application of an LC-MS/MS Method for Reliable Determination of Amodiaquine, N-Desethylamodiaquine, Artesunate and Dihydroartemisinin in Human Plasma for a Bioequivalence Study in Healthy Indian Subjects," *Journal of Pharmaceutical and Biomedical Analysis* 124 (2016): 67–78, https://doi.org/10.1016/j.jpba.2016.02.021.

[8] E. Kokori, G. Olatunji, A. Akinboade, et al., "Triple Artemisinin-Based Combination Therapy (TACT): Advancing Malaria Control and Eradication Efforts," *Malaria Journal* 23, no. 1 (2024): 25–27, https://doi.org/10.1186/s12936-024-04844-y.

[9] T. D. Nguyen, B. Gao, C. Amaratunga, et al., "Preventing Antimalarial Drug Resistance With Triple Artemisinin-Based Combination Therapies," *Nature Communications* 14, no. 1 (2023): 4568, https://doi.org/10.1038/s41467-023-39914-3.

[10] M. Ndounga, P. I. Mayengue, R. Tahar, et al., "Efficacy of Sulfadoxine-Pyrimethamine, Amodiaquine, and Sulfadoxine-Pyrimethamine–Amodiaquine Combination for the Treatment of Uncomplicated Falciparum Malaria in the Urban and Suburban Areas of Brazzaville (Congo)," *Acta Tropica* 103, no. 3 (2007): 163–171, https://doi.org/10.1016/j.actatropica.2007.06.002.

[11] E. N. U. Ezedinachi, O. J. Ekanem, C. M. Chukwuani, et al., "Efficacy and Tolerability of a Low-Dose Mefloquine-Sulfadoxine- Pyrimethamine Combination Compared with Chloroquine in the Treatment of Acute Malaria Infection in a Population with Multiple Drug-Resistant Plasmodium Falciparum," *The American Journal of Tropical Medicine and Hygiene* 61, no. 1 (1999): 114–119, https://doi.org/10.4269/ajtmh.1999.61.114.

[12] S. G. Staedke, M. R. Kamya, G. Dorsey, et al., "Amodiaquine, Sulfadoxine/pyrimethamine, and Combination Therapy for Treatment of Uncomplicated Falciparum Malaria in Kampala, Uganda: A Randomised Trial," *Lancet (London, England)* 358, no. 9279 (2001): 368–374, https://doi.org/10.1016/S0140-6736(01)05557-X.

[13] T. D. Clark, D. Njama-Meya, B. Nzarubara, et al., "Incidence of Malaria and Efficacy of Combination Antimalarial Therapies Over 4 Years in an Urban Cohort of Ugandan Children," *PLoS One* 5, no. 7 (2010): 117599–e11768, https://doi.org/10.1371/journal.pone.0011759.

[14] R. J. Maude, D. Socheat, C. Nguon, et al., "Optimising Strategies for Plasmodium Falciparum Malaria Elimination in Cambodia: Primaquine, Mass Drug Administration and Artemisinin Resistance," *PLoS One* 7, no. 5 (2012): e37166, https://doi.org/10.1371/journal.pone.0037166.

[15] N. J. White and K. Chotivanich, "Artemisinin-Resistant Malaria," *Clinical Microbiology Reviews* 37, no. 4 (2024): e0010924, https://doi.org/10.1128/cmr.00109-24.

[16] N. J. White, "Can New Treatment Developments Combat Resistance in Malaria?" *Expert Opinion on Pharmacotherapy* 17, no. 10 (2016): 1303–1307, https://doi.org/10.1080/14656566.2016.1187134.

[17] J. L. Siqueira-Neto, K. J. Wicht, K. Chibale, J. N. Burrows, D. A. Fidock, and E. A. Winzeler, "Antimalarial Drug Discovery: Progress and Approaches," *Nature Reviews Drug Discovery* 22, no. 10 (2023): 807–826, https://doi.org/10.1038/s41573-023-00772-9.

[18] B. M. Eales, C. S. Hudson, I. Kesisoglou, W. Wang, M. Nikolaou, and V. H. Tam, "Experimental Validation of a Mathematical Framework to Simulate Antibiotics With Distinct Half-Lives Concurrently in an In Vitro Model," *Antibiotics* 10, no. 10 (2021): 1256, https://doi.org/10.3390/antibiotics10101256.

[19] G. D. Shanks, M. D. Edstein, and D. Jacobus, "Evolution From Double to Triple-Antimalarial Drug Combinations," *Transactions of the Royal Society of Tropical Medicine and Hygiene* 109, no. 3 (2014): 182–188, https://doi.org/10.1093/trstmh/tru199.

[20] G. R. Rocha, F. F. B. Lemos, L. G. d. O. Silva, et al., "Overcoming Antibiotic-Resistant Helicobacter Pylori Infection: Current Challenges and Emerging Approaches," *World Journal of Gastroenterology* 31, no. 10 (2025): 1–24, https://doi.org/10.3748/wjg.v31.i10.102289.

[21] S. Ramteke, N. Ganesh, S. Bhattacharya, and N. K. Jain, "Triple Therapy-Based Targeted Nanoparticles for the Treatment of *Helicobacter pylori*," *Journal of Drug Targeting* 16, no. 9 (2008): 694–705, https://doi.org/10.1080/10611860802295839.

[22] E. J. Arts, D. J. Hazuda, E. F. D. Bushman, G. J. Nabel, and R. Swanstrom, "HIV-1 Antiretroviral Drug Therapy Basic Principles of Antiretroviral Ir," *Cold Spring Harbor Perspectives in Medicine* 2, no. a007161 (2012): 1–23.

[23] J. P. Freeling, J. Koehn, C. Shu, J. Sun, and R. J. Y. Ho, "Anti-HIV Drug-Combination Nanoparticles Enhance Plasma Drug Exposure Duration as Well as Triple-Drug Combination Levels in Cells within Lymph Nodes and Blood in Primates," *AIDS Research and Human Retroviruses* 31, no. 1 (2015): 107–114, https://doi.org/10.1089/aid.2014.0210.

[24] G. Martínez-Edo, E. Y. Xue, S. Y. Y. Ha, et al., "Nanoparticles for Triple Drug Release for Combined Chemo- and Photodynamic Therapy," *Chemistry-A European Journal* 27, no. 59 (2021): 14610–14618, https://doi.org/10.1002/chem.202101842.

[25] M. T. Ansari, K. T. Batty, I. Iqbal, and V. B. Sunderland, "Improving the Solubility and Bioavailability of Dihydroartemisinin by Solid Dispersions and Inclusion Complexes," *Archives of Pharmacal Research* 34, no. 5 (2011): 757–765, https://doi.org/10.1007/s12272-011-0509-1.

[26] E. A. Ashley, J. Recht, and N. J. White, "Primaquine: The Risks and the Benefits," *Malaria Journal* 13, no. 1 (2014): 418–427, https://doi.org/10.1186/1475-2875-13-418.

[27] J. N. Burrows, S. Duparc, W. E. Gutteridge, et al., "New Developments in Anti-malarial Target Candidate and Product Profiles," *Malaria Journal* 16, no. 1 (2017): 26–29, https://doi.org/10.1186/s12936-016-1675-x.

[28] A. Martinelli, R. Moreira, and P. Cravo, "Malaria Combination Therapies: Advantages and Shortcomings," *Mini-Reviews in Medicinal Chemistry* 8, no. 3 (2008): 201–212, https://doi.org/10.2174/138955708783744092.

[29] O. Abdifetah and K. Na-Bangchang, "Pharmacokinetic Studies of Nanoparticles as a Delivery System for Conventional Drugs and Herb-Derived Compounds for Cancer Therapy: A Systematic Review," *International Journal of Nanomedicine* 14 (2019): 5659–5677, https://doi.org/10.2147/IJN.S213229.

[30] S. B. Lim, A. Banerjee, and H. Önyüksel, "Improvement of Drug Safety by the Use of Lipid-Based Nanocarriers," *Journal of Controlled Release* 163, no. 1 (2012): 34–45, https://doi.org/10.1016/j.jconrel.2012.06.002.

[31] L. N. Kekani and B. A. Witika, "Current Advances in Nanodrug Delivery Systems for Malaria Prevention and Treatment," *Discover Nano* 18, no. 1 (2023): 66, https://doi.org/10.1186/s11671-023-03849-x.

[32] K. Shakeel, S. Raisuddin, S. Ali, et al., "Development and In Vitro/In Vivo Evaluation of Artemether and Lumefantrine Co-loaded Nanoliposomes for Parenteral Delivery," *Journal of Liposome Research* 29, no. 1 (2019): 35–43, https://doi.org/10.1080/08982104.2017.1410173.

[33] P. Severino, T. Andreani, A. S. Macedo, et al., "Current State-Of-Art and New Trends on Lipid Nanoparticles (SLN and NLC) for Oral Drug Delivery," *Journal of Drug Delivery* 2012 (2012): 1–10, https://doi.org/10.1155/2012/750891.

[34] J. O. Muga, J. W. Gathirwa, M. Tukulula, and W. G. Z. O. Jura, "In Vitro Evaluation of Chloroquine-Loaded and Heparin Surface-Functionalized Solid Lipid Nanoparticles," *Malaria Journal* 17 (2018): 133–137, https://doi.org/10.1186/s12936-018-2302-9.

[35] G. Pradel, S. Garapaty, and U. Frevert, "Proteoglycans Mediate Malaria Sporozoite Targeting to the Liver," *Molecular Microbiology* 45, no. 3 (2002): 637–651, https://doi.org/10.1046/j.1365-2958.2002.03057.x.

[36] Y. Avalos-Padilla and X. Fernàndez-Busquets, "Nanotherapeutics against Malaria: A Decade of Advancements in Experimental Models," *WIREs Nanomedicine and Nanobiotechnology* 16, no. 2 (2024): 1–28, https://doi.org/10.1002/wnan.1943.

[37] J. M. Ms, E. M. Ms, P. Urbán, et al., "Application of Heparin as a Dual Agent With Antimalarial and Liposome Targeting Activities Towards Plasmodium-Infected Red Blood Cells," *Nanomedicine: Nanotechnology, Biology and Medicine* (2014): https://doi.org/10.1016/j.nano.2014.06.002.

[38] P. B. Lokole, G. G. Byamungu, P. K. Mutwale, et al., "Plant-Based Nanoparticles Targeting Malaria Management," *Frontiers in Pharmacology* 15 (2024): 1440116–1440126, https://doi.org/10.3389/fphar.2024.1440116.

[39] K. K. Singh and S. K. Vingkar, "Formulation, Antimalarial Activity and Biodistribution of Oral Lipid Nanoemulsion of Primaquine," *International Journal of Pharmaceutics* 347, no. 1–2 (2008): 136–143, https://doi.org/10.1016/j.ijpharm.2007.06.035.

[40] W. N. Omwoyo, P. Melariri, J. W. Gathirwa, et al., "Development, Characterization and Antimalarial Efficacy of Dihydroartemisinin Loaded Solid Lipid Nanoparticles," *Nanomedicine: Nanotechnology, Biology and Medicine* 12, no. 3 (2016): 801–809, https://doi.org/10.1016/j.nano.2015.11.017.

[41] S. E. Haas, C. C. Bettoni, L. K. de Oliveira, S. S. Guterres, and T. Dalla Costa, "Nanoencapsulation Increases Quinine Antimalarial Efficacy Against Plasmodium Berghei In Vivo," *International Journal of Antimicrobial Agents* 34, no. 2 (2009): 156–161, https://doi.org/10.1016/j.ijantimicag.2009.02.024.

[42] P. B. Memvanga and C. I. Nkanga, "Liposomes for Malaria Management: the Evolution from 1980 to 2020," *Malaria Journal* 20, no. 1 (2021): 327–333, https://doi.org/10.1186/s12936-021-03858-0.

[43] V. Kumari, A. Sangal, and R. Mehta, "In Vitro Kinetic Release Study of terminalia Arjuna Loaded PLGA Nanoparticles," *Trends in Biomaterials and Artificial Organs* 35, no. 1 (2021): 10–14.

[44] S. Desgouilles, C. Vauthier, D. Bazile, et al., "The Design of Nanoparticles Obtained by Solvent Evaporation: A Comprehensive Study," *Langmuir* 19, no. 22 (2003): 9504–9510, https://doi.org/10.1021/la034999q.

[45] ICH, "International Conference on Harmonization (ICH). Guidance for Industry: Q1A(R2) Stability Testing of New Drug Substances and Products," *Ich Harmonised Tripartite Guideline* 4 (2003): 24.

[46] W. N. Omwoyo, B. Ogutu, F. Oloo, et al., "Preparation, Characterization, and Optimization of Primaquine-Loaded Solid Lipid Nanoparticles," *International Journal of Nanomedicine* 9, no. 1 (2014): 3865–3874, https://doi.org/10.2147/IJN.S62630.

[47] Y. Gao, J. Zuo, N. Bou-Chacra, et al., "In Vitro Release Kinetics of Antituberculosis Drugs from Nanoparticles Assessed Using a Modified Dissolution Apparatus," *BioMed Research International* 2013 (2013): 1–9, https://doi.org/10.1155/2013/136590.

[48] K. Torres-Rivero, J. Bastos-Arrieta, N. Fiol, and A. Florido, "Metal and Metal Oxide Nanoparticles: An Integrated Perspective of the Green Synthesis Methods by Natural Products and Waste Valorization: Applications and Challenges," *Comprehensive Analytical Chemistry* 94 (2021): 433–469, https://doi.org/10.1016/bs.coac.2020.12.001.

[49] V. Thiruvengadam and A. V. Bansod, "Characterization of Silver Nanoparticles Synthesized Using Chemical Method and Its Antibacterial Property," *Biointerface Research in Applied Chemistry* 10, no. 6 (2020): 7257–7264, https://doi.org/10.33263/BRIAC106.72577264.

[50] W. Peters, "Drug Resistance in Plasmodium Berghei. I. Chloroquine Resistance," *Experimental Parasitology* 17, no. 1 (1965): 80–89, https://doi.org/10.1016/0014-4894(65)90012-3.

[51] K. Nyandwaro, J. Oyweri, F. Kimani, and A. Mbugua, "Evaluating Antiplasmodial and Antimalarial Activities of Soybean (Glycine Max) Seed Extracts on *P. falciparum* Parasite Cultures and *P. berghei*-Infected Mice," *Journal of Pathogens* 2020 (2020): 1–8, https://doi.org/10.1155/2020/7605730.

[52] P. A. Odera, G. Otieno, J. O. Onyango, et al., "Nanoparticle-Based Formulation of Dihydroartemisinin-Lumefantrine Duo-Drugs: Preclinical Evaluation and Enhanced Antimalarial Efficacy in a Mouse Model," *Heliyon* 10, no. 6 (2024): e26868, https://doi.org/10.1016/j.heliyon.2024.e26868.

[53] P. Nath and A. Yadav, "Acute and Sub-Acute Oral Toxicity Assessment of the Methanolic Extract From Leaves of Hibiscus Rosa-Sinensis L. In Mice," *Journal of Intercultural Ethnopharmacology* 4, no. 1 (2015): 70, https://doi.org/10.5455/jice.20141028021746.

[54] N. S. Njinga, A. T. Kola-mustapha, A. L. Quadri, et al., "Toxicity Assessment of Sub-Acute and Sub-Chronic Oral Administration and Diuretic Potential of Aqueous Extract of

Hibiscus sabdariffa Calyces," *Heliyon* 6, no. 9 (2020): e04853, https://doi.org/10.1016/j.heliyon.2020.e04853.

[55] S. E. Lazic, E. Semenova, and D. P. Williams, "Determining Organ Weight Toxicity with Bayesian Causal Models: Improving on the Analysis of Relative Organ Weights," *Scientific Reports* 10, no. 1 (2020): 6625–6712, https://doi.org/10.1038/s41598-020-63465-y.

[56] R. Mačianskienė, V. Zigmantaitė, I. Andriulė, et al., "Acute and Sub-chronic Intraperitoneal Toxicity Studies of the Elsholtzia Ciliata Herbal Extract in Balb/c Mice," *Pharmaceutics* 15, no. 10 (2023): 2417, https://doi.org/10.3390/pharmaceutics15102417.

[57] C. Liu, X. Jiang, Y. Gan, and M. Yu, "Engineering Nanoparticles to Overcome the Mucus Barrier for Drug Delivery: Design, Evaluation and State-Of-The-Art," *Medicine in Drug Discovery* 12 (2021): 100110, https://doi.org/10.1016/j.medidd.2021.100110.

[58] E. Blanco, H. Shen, and M. Ferrari, "Principles of Nanoparticle Design for Overcoming Biological Barriers to Drug Delivery," *Nature Biotechnology* 33, no. 9 (2015): 941–951, https://doi.org/10.1038/nbt.3330.

[59] X. Yang, H. Du, J. Liu, and G. Zhai, "Advanced Nanocarriers Based on Heparin and its Derivatives for Cancer Management," *Biomacromolecules* 16, no. 2 (2015): 423–436, https://doi.org/10.1021/bm501532e.

[60] M. A. Dobrovolskaia, P. Aggarwal, J. B. Hall, and S. E. McNeil, "Preclinical Studies to Understand Nanoparticle Interaction With the Immune System and its Potential Effects on Nanoparticle Biodistribution," *Molecular Pharmaceutics* 5, no. 4 (2008): 487–495, https://doi.org/10.1021/mp800032f.

[61] T. Marante, C. Viegas, I. Duarte, A. S. Macedo, and P. Fonte, "An Overview on Spray-Drying of Protein-Loaded Polymeric Nanoparticles for Dry Powder Inhalation," *Pharmaceutics* 12, no. 11 (2020): 1032–1123, https://doi.org/10.3390/pharmaceutics12111032.

[62] X. Zhang, J. Liu, H. Qiao, et al., "Formulation Optimization of Dihydroartemisinin Nanostructured Lipid Carrier Using Response Surface Methodology," *Powder Technology* 197, no. 1–2 (2010): 120–128, https://doi.org/10.1016/j.powtec.2009.09.004.

[63] S. Dash, P. N. Murthy, L. Nath, and P. Chowdhury, "Kinetic Modeling on Drug Release from Controlled Drug Delivery Systems," *Acta Poloniae Pharmaceutica* 67, no. 3 (2010): 217–223.

[64] I. S. Bayer, "Controlled Drug Release from Nanoengineered Polysaccharides," *Pharmaceutics* 15, no. 5 (2023): 1364, https://doi.org/10.3390/pharmaceutics15051364.

[65] H. Baishya, "Application of Mathematical Models in Drug Release Kinetics of Carbidopa and Levodopa ER Tablets," *Journal of Developing Drugs* 06, no. 02 (2017): 1–8, https://doi.org/10.4172/2329-6631.1000171.

[66] F. Haghiralsadat, G. Amoabediny, M. N. Helder, et al., "A Comprehensive Mathematical Model of Drug Release Kinetics From Nano-Liposomes, Derived from Optimization Studies of Cationic PEGylated Liposomal Doxorubicin Formulations for Drug-Gene Delivery," *Artificial Cells, Nanomedicine and Biotechnology* 46, no. 1 (2018): 169–177, https://doi.org/10.1080/21691401.2017.1304403.

[67] R. Kumar, A. Singh, N. Garg, and P. F. Siril, "Solid Lipid Nanoparticles for the Controlled Delivery of Poorly Water Soluble Non-steroidal Anti-inflammatory Drugs," *Ultrasonics Sonochemistry* 40 (2018): 686–696, https://doi.org/10.1016/j.ultsonch.2017.08.018.

[68] F. Nasiri, L. Faghfouri, and M. Hamidi, "Preparation, Optimization, And*in-Vitro*characterization of α-Tocopherol-loaded Solid Lipid Nanoparticles (SLNs)," *Drug Development and Industrial Pharmacy* 46, no. 1 (2020): 159–171, https://doi.org/10.1080/03639045.2019.1711388.

[69] Y. Liu, G. Yang, S. Jin, L. Xu, and C. X. Zhao, "Development of High-Drug-Loading Nanoparticles," *ChemPlusChem* 85, no. 9 (2020): 2143–2157, https://doi.org/10.1002/cplu.202000496.

[70] Z. Yang, H. Peng, W. Wang, and T. Liu, "Crystallization Behavior of Poly (ε-Caprolactone)/Layered Double Hydroxide Nanocomposites," *Journal of Applied Polymer Science* 116, no. 5 (2010): 2658–2667, https://doi.org/10.1002/app.

[71] D. S. Villarreal-Lucio, J. L. Rivera Armenta, I. A. Estrada Moreno, and R. Garcia-Alamilla, "Effect of Surfactant in Particle Shape and Thermal Degradation of Eggshell Particles," *Materials Research* 22, no. 3 (2019): https://doi.org/10.1590/1980-5373-MR-2018-0778.

[72] M. F. Queiroz, K. R. T. Melo, D. A. Sabry, G. L. Sassaki, and H. A. O. Rocha, "Does the Use of Chitosan Contribute to Oxalate Kidney Stone Formation?" *Marine Drugs* 13, no. 1 (2015): 141–158, https://doi.org/10.3390/md13010141.

[73] C. Song, H. Yu, M. Zhang, Y. Yang, and G. Zhang, "Physicochemical Properties and Antioxidant Activity of Chitosan From the Blowfly *Chrysomya megacephala* Larvae," *International Journal of Biological Macromolecules* 60 (2013): 347–354, https://doi.org/10.1016/j.ijbiomac.2013.05.039.

[74] S. Jain, S. K. Jain, P. Khare, A. Gulbake, D. Bansal, and S. K. Jain, "Design and Development of Solid Lipid Nanoparticles for Topical Delivery of an Anti-Fungal Agent," *Drug Delivery* 17, no. 6 (2010): 443–451, https://doi.org/10.3109/10717544.2010.483252.

[75] E. Rostami, S. Kashanian, and M. Askari, "The Effect of Ultrasound Wave on Levothyroxine Release From Chitosan Nanoparticles," *Advanced Materials Research* 829 (2013): 284–288, https://doi.org/10.4028/www.scientific.net/amr.829.284.

[76] S. U. Rahman, S. Bilal, and A. U. H. Ali Shah, "Synthesis and Characterization of Polyaniline-Chitosan Patches With Enhanced Stability in Physiological Conditions," *Polymers* 12, no. 12 (2020): 1–13, https://doi.org/10.3390/polym12122870.

[77] S. Glushakova, B. L. Busse, M. Garten, et al., "Exploitation of a Newly-Identified Entry Pathway Into the Malaria Parasite-Infected Erythrocyte to Inhibit Parasite Egress," *Scientific Reports* 7, no. 1 (2017): 12250–12313, https://doi.org/10.1038/s41598-017-12258-x.

[78] P. Prabhu, S. Suryavanshi, S. Pathak, S. Sharma, and V. Patravale, "Artemether–lumefantrine Nanostructured Lipid Carriers for Oral Malaria Therapy: Enhanced Efficacy at Reduced Dose and Dosing Frequency," *International Journal of Pharmaceutics* 511, no. 1 (2016): 473–487, https://doi.org/10.1016/j.ijpharm.2016.07.021.

[79] X. Zhou, F. Suo, K. Haslinger, and W. J. Quax, "Artemisinin-Type Drugs in Tumor Cell Death: Mechanisms, Combination Treatment With Biologics and Nanoparticle Delivery," *Pharmaceutics* 14, no. 2 (2022): 395, https://doi.org/10.3390/pharmaceutics14020395.

[80] S. Samat, N. A. Nor, F. Nor Hussein, W. I. W. Ismail, and W. Ismail, "Effects of Gelam and Acacia Honey Acute Administration on Some Biochemical Parameters of Sprague Dawley Rats," *BMC Complementary and Alternative Medicine* 14, no. 1 (2014): 146, https://doi.org/10.1186/1472-6882-14-146.

[81] S. Teo, D. Stirling, S. Thomas, A. Hoberman, A. Kiorpes, and V. Khetani, "A 90-day Oral Gavage Toxicity Study of D-

Methylphenidate and D,L-Methylphenidate in Sprague-Dawley Rats," *Toxicology* 179, no. 3 (2002): 183–196, https://doi.org/10.1016/S0300-483X(02)00338-4.

[82] Y. S. Ong, L. Saiful Yazan, W. K. Ng, et al., "Acute and Subacute Toxicity Profiles of Thymoquinone-Loaded Nanostructured Lipid Carrier in BALB/c Mice," *International Journal of Nanomedicine* 11 (2016): 5905–5915, https://doi.org/10.2147/IJN.S114205.

[83] A. Kasiti Muganda, E. O. Okonjo, J. Nyabuga Nyariki, et al., "Schistosoma Mansoni Co-Infection Decelerates Murine Plasmodium Berghei ANKA Induced Inflammatory Response and Organ Damage," *American Journal of Infectious Diseases and Microbiology* 10, no. 2 (2022): 58–69, https://doi.org/10.12691/ajidm-10-2-2.